الجمهورية الجزائرية الديمقراطية الشعبية

People's Democratic Republic of Algeria

Ministry of Higher Education and Scientific Research

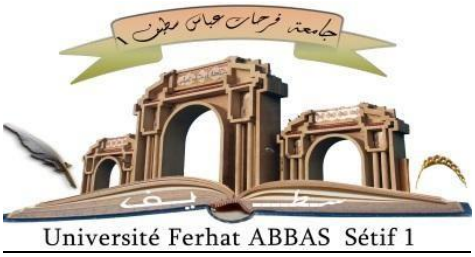

Ferhat Abbas University Setif 1

Faculty of Technology

THESIS

Presented to the Process Engineering Department

For obtaining the diploma of:

DOCTORATE

Domain: Science and Technology

Field: Process Engineering **Option:** Polymer Engineering

By

REGUIG Abdelbasset Abdessamed

THEME

Effect of Diatomaceous earth filler and Reversible Crosslinking Reaction Agent (RXR) on High-Density Polyethylene (HDPE) and Isotactic Polybutene (PB-1)

Defended on: 09/11/2024, In front of the jury:

BENANIBA Mohamed Tahar	**Professor**	**Ferhat Abbas University Setif 1**	**President**
BOUHELAL Said	**Professor**	**Ferhat Abbas University Setif 1**	**Supervisor**
RIAHI Faird	**Professor**	**Ferhat Abbas University Setif 1**	**Examiner**
HAMMA Amel	**M.C.A**	**Med El Bachir El Ibrahimi University BBA**	**Examiner**
DOUFNOUNE Rachida	**Professor**	**Ferhat Abbas University Setif 1**	**Invited**

الجمهورية الجزائرية الديمقراطية الشعبية

République Algérienne Démocratique et Populaire

Ministère de L'Enseignement Supérieur et de la Recherche Scientifique

Université Ferhat ABBAS Sétif 1

Université Ferhat Abbas Sétif 1

Faculté de Technologie

THESE

Présentée au Département de Génie des Procèdes

Pour l'obtention du diplôme de

DOCTORAT

Domaine: Sciences et Technologie

Filière : Génie des Procédés **Option** : Génie des Polymères

Par

REGUIG Abdelbasset Abdessamed

THÈME

Effet de la Diatomite et de l'agent de réaction de réticulation réversible (RXR) sur le Polyéthylène Haute-Densité (HDPE) et le Polybutène isotactique (PB-1)

Soutenue le : 09/11/2024, devant le Jury :

BENANIBA Mohamed Tahar	**Professeur**	**Univ. Ferhat Abbas Sétif 1**	**Président**
BOUHELAL Said	**Professeur**	**Univ. Ferhat Abbas Sétif 1**	**Directeur de thèse**
RIAHI Faird	**Professeur**	**Univ. Ferhat Abbas Sétif 1**	**Examinateur**
HAMMA Amel	**M.C.A**	**Univ. Med El Bachir El Ibrahimi BBA**	**Examinatrice**
DOUFNOUNE Rachida	**Professeur**	**Univ. Ferhat Abbas Sétif 1**	**Membre Invité**

ACKNOWLEDGEMENTS

My first and last gratitude go to the almighty Allah, for giving me the will and the strength to pursue this beautiful dream instead of the hardship and all the obstacles faced along the way, for the guidance, the knowledge and wisdom acquired during these past years and for academic companionship that has a tremendous impact on my doctoral journey.

To Professors **BOUHELAL** and **DOUFNOUNE**, my deepest and sincere gratitude to you two for your efforts, help, guidance and the knowledge you shared with us not only during the doctorate, but also in the previous years as your students.

I also want to thank the jury members for accepting our invitation to judge and evaluate our work and undoubtedly enrich it giving their profound knowledge in the field of polymers, polymeric composites and nanotechnology science.

Lastly, I want to thank my fellow researchers who have the bigger part of the credit for completing this thesis after the mighty Allah. To you my dear Doctor friends: **Dr. Aoussi Tahar, Dr. Kabache Fayçal,** and **Dr. Benayache Walid**, thank you from the bottom of my heart for all the help you provided me with, for both the emotional and physical help and for everything else, even a smile or a simple kind word.

DEDICATIONS

This Doctorate status and diploma is dedicated to the two dearest and most precious people to my heart on this planet, the reason of my existence in the first place, my dear Parents, May Allah extend your life and keep you safe from any harm, healthy and beside me till the mighty Allah takes back my soul.

I also want to dedicate this work to my beloved friends, to my second school, the **ENPC GROUP**. Huge thanks to **Mr. HASSAD** and **Mr. LOUCIF** for their help and guidance in my professional carrier and to all those who believed in me and wished me success.

Last but not least, I want to dedicate this work to **Me** and I want to thank **Me** for believing in **Me** and being there for **Me** in the bad and good and sad and happy days.

TABLE OF CONTENTS

FIGURES LIST

CHAPTER I

CHAPTER II

CHAPTER III

CHAPTER IV

TABLES LIST

CHAPTER II

CHAPTER III

CHAPTER IV

LIST OF ABBREVIATIONS AND SYMBOLS

HDPE	High Density Polyethylene
PB-1	Isotactic Polybutene-1
S8	Sulfur
TMTD	Tetramethyl Thiuram Disulfide
DCP	Dicumyl peroxide
DSC	Differential Scanning Calorimetry
TGA	Thermogravimetric Analysis
DRA	Dynamic Rheological Analysis
FTIR	Fourier Transform Infrared
WAXS	Wide-Angle X-ray scattering
SEM	Scanning Electron Microscope
RXR	Reversible Crosslinking Reaction
σ_f	Stress at failure
ε_f	Strain at failure
$\sigma_{0.2y}$	0.2% offset yield stress
$\varepsilon_{0.2y}$	0.2% offset yield strain
σ_{UTS}	Ultimate tensile strength
ε_{UTS}	Ultimate tensile strain
E	Young's modulus (Stiffness)
I	Impact resistance
T_0	Initial decomposition temperature
T_f	Final decomposition temperature
T_{50}	Decomposition temperature at 50% weight loss
dwt	Weight loss rate
T_{DTG}	Temperature at the highest decomposition rate
T_{m1}	Melting temperature in the first heating cycle
T_{m2}	Melting temperature in the second heating cycle
ΔH_{m1}	Enthalpy of fusion of the first melting peak
ΔH_{m2}	Enthalpy of fusion of the second melting peak
ΔH_c	Enthalpy of Crystallization
Xc_1	Degree of crystallinity of the first heating cycle
Xc_2	Degree of crystallinity of the second heating cycle
T_{m0}	Melting onset temperature
T_m	Maximum melting temperature
ΔH_m	Enthalpy of fusion
T_{c0}	Crystallization onset temperature
T_c	Maximum Crystallization temperature
X_c	Degree of crystallinity
L_c	Lamellar thickness
β	full width at half maximum
L	Crystallite size
d	Inter planar spacing

GENERAL INTRODUCTION

GENERAL INTRODUCTION

Since the advent of plastics in the early 1933s, researchers from academia and the petrochemical industry have been competing to create novel polymers with diverse properties to meet market demands while keeping costs low. The most often used approach for chemically synthesizing polymers is polymerization, which involves beginning from a building block called a 'monomer'. The growing demand for polymeric materials has led to a large growth in the demand for highly specialized polymers with specific characteristics. As a result, the scientific community has been compelled to devise innovative methods for the production of these polymers. By utilizing chemistry, it became feasible to construct polymers with desired properties by deliberately incorporating particular types of molecules in a controlled manner through copolymerization techniques. This process leads to the creation of a polymer that combines the characteristics of two or more polymers that have been mixed together. This result has significantly advantaged humanity and resolved various types of issues that were prevalent in the market. In addition, like the polymerization reaction, this approach also suffers from the disadvantages of being complex and expensive [1]. Polymer blending, the inclusion of fillers into the polymers to create a composite material, or even chemically modifying the molecular chains by functionalization or crosslinking are all cost-effective methods to alter the end properties of the polymer. Blending binary, tertiary, or even more polymers together is a cost-effective way to combine the performances of the component polymers, or at least to get the properties of one of them in comparison to polymerization or the copolymerization method [2]. The technique of reinforcing polymeric materials with organic or inorganic substances of varying sizes is widely used to modify their properties, flow characteristics, and reduce expenses. Additionally, if the filler particles are effectively dispersed and bonded to the polymer chains, this technique can also enhance the mechanical, thermal, and barrier properties of the materials [2, 3].

High-Density Polyethylene (HDPE) has long been recognized as a highly popular and widely utilized polymer because to its exceptional characteristics, including impressive tensile strength, rigidity, resistance to chemicals, lightweight nature, ease of processing, and resistance to both chemicals and water. Additionally, it is renowned for its ability to be recycled, its affordability, its adaptability, its durability, and numerous other characteristics [3, 4]. Polybutene-1 (PB-1) is a polymorphic polymer with a high molecular weight and a chemical structure that is similar to polypropylene (PP). It possesses an isotactic and semi-crystalline structure [1]. PB-1, similar to other polyolefins, exhibits favorable chemical resistance, resistance to environmental stress cracking, and notably, exceptional

creep qualities even under high temperatures. It also demonstrates outstanding flexibility and elasticity, resistance to abrasion, and strong puncture resistance when used in film applications [5–11], It is an excellent option for products that need to be highly durable, such as pressurized tanks and plumbing pipes for hot and cold water. This is particularly true for pressurized pipes that come into contact with chlorinated water, as they have a longer lifespan compared to regular polyolefin pipes. Additionally, it is suitable for technical products like easy-to-peel packaging for cereals, coffee powder, meat, and frozen foods storage, as well as hot melt adhesives [12, 13]. A wide variety of fillers, which can be either naturally obtained or artificially produced, are employed in polymeric materials as functional modifiers or as inert fillers to decrease the cost of the final product. Diatomite, also referred to as diatomaceous earth or kieselguhr [14, 15] , is a specific category of fillers. Hydrated amorphous silica (SiO_2, nH_2O) is a substance with a structure consisting of water molecules and silicon dioxide. It has a size of a few tens of micrometers. This substance is known for its exceptional characteristics, including being lightweight, having low density, being resistant to chemicals, having a large surface area, being able to withstand high temperatures, and having high porosity. As a result, it has become widely used in various industries such as food, cosmetics, pharmaceuticals, petroleum, chemicals, coatings, plastics, and rubber [16]. Due to its porous structure, high surface area, and excellent chemical resistance, it serves as an effective filtration medium for various organic and inorganic substances [17, 18]. Given its nanoscale pore size [19] and mostly silica composition, it was considered a promising nanofiller option for polymeric materials [20–22].

The present thesis explores the effect of the Diatomaceous earth filler and the reversible crosslinking reaction agent (RXR) on two types of polyolefin polymers, High density polyethylene and Isotactic polybutene-1 (PB-1). Various characterization methods were employed to examine the rheological, mechanical, thermal, structural and morphological characteristics of HDPE/Diatomaceous earth and PB-1/Diatomaceous earth microcomposites, both in the absence and the presence of the RXR agent. Diatomaceous earth filler was employed seeking the improvement of the thermal stability and the mechanical properties of the both polymers if possible. Meanwhile, the purpose from the inclusion of the RXR agent into both composites systems, was to investigate its effect on the dispersion of the filler and the possible surface modification of the later, resulting in a possible improvement of the mechanical properties and structure modification in the case of PB-1.

The present thesis was divided into four main chapters, as follow:

Chapter I: A literature review on polyolefins, composite materials and specifically diatomite-based composites and polymer chemical modification;

Chapter II: Describes the materials used, the preparation methods and the various techniques used during characterization;

Chapter III: Investigate the Enhancement of High-Density Polyethylene (HDPE) Performance with Diatomaceous earth filler and a Novel Reversible Crosslinking Reaction Agent (RXR);

Chapter IV: Studies the Improving isotactic polybutene-1 (PB-1) performance with Diatomaceous earth filler and a novel reversible crosslinking reaction agent (RXR).

Finally, we conclude our work with a general conclusion and perspectives.

REFERENCES

[1] Kutz, M. *Applied Plastics Engineering Handbook, Processing, Materials, and Applications*, 2nd ed.; Kutz, M., Ed.; William Andrew Publications. https://doi.org/10.1016/C2014-0-04118-4.

[2] Zhang, Q.; Khan, M. U.; Lin, X.; Cai, H.; Lei, H. Temperature Varied Biochar as a Reinforcing Filler for High-Density Polyethylene Composites. *Compos. B Eng.* **2019**, *175*, 107151. https://doi.org/10.1016/j.compositesb.2019.107151.

[3] Li, Y.; Li, D.; Cheng, H.; Han, C.; Xiao, L. Morphology and Physical Properties of Composites Based on High-Density Polyethylene/Propylene-Ethylene Random Copolymers Blends and Carbon Black. *Polym. Test.* **2023**, *123*, 108050. https://doi.org/10.1016/j.polymertesting.2023.108050.

[4] Ronca, S. Polyethylene. In *Brydson's Plastics Materials*; Elsevier, 2017; pp 247–278. https://doi.org/10.1016/B978-0-323-35824-8.00010-4.

[5] Hu, D.; Li, W.; Wu, K.; Cui, L.; Xu, Z.; Zhao, L. Utilization of Supercritical CO2 for Controlling the Crystal Phase Transition and Cell Morphology of Isotactic Polybutene-1 Foams. *J. CO2 Util.* **2022**, *66*, 102265. https://doi.org/10.1016/j.jcou.2022.102265.

[6] Lundbäck, M.; Hassinen, J.; Andersson, U.; Fujiwara, T.; Gedde, U. W. Polybutene-1 Pipes Exposed to Pressurized Chlorinated Water: Lifetime and Antioxidant Consumption. *Polym. Degrad. Stab.* **2006**, *91* (4), 842–847. https://doi.org/10.1016/j.polymdegradstab.2005.06.015.

[7] Afrifah, K. A.; Hickok, R. A.; Matuana, L. M. Polybutene as a Matrix for Wood Plastic Composites. *Compos. Sci. Technol.* **2010**, *70* (1), 167–172. https://doi.org/10.1016/j.compscitech.2009.09.019.

[8] Andena, L.; Rink, M.; Frassine, R.; Corrieri, R. A Fracture Mechanics Approach for the Prediction of the Failure Time of Polybutene Pipes. *Eng. Fract. Mech.* **2009**, *76* (18), 2666–2677. https://doi.org/10.1016/j.engfracmech.2009.10.002.

[9] Schoßig, M.; Grellmann, W.; Mecklenburg, T. Characterization of the Fracture Behavior of Glass Fiber Reinforced Thermoplastics Based on PP, PE-HD, and PB-1. *J. Appl. Polym. Sci.* **2010**, *115* (4), 2093–2102. https://doi.org/10.1002/app.31271.

[10] Yang, X.; Dong, B.; Shang, Y.; Ji, Y.; Su, F.; Shao, C.; Wang, Y.; Liu, C.; Shen, C. Investigation on the Phase Transition from Form II to Form I in IPB-1 after Pre-Stretching. *Polymer (Guildf.)* **2020**, *194*, 122385. https://doi.org/10.1016/j.polymer.2020.122385.

[11] Zhang, Z.; Chen, X.; Zhang, C.; Liu, C.-T.; Wang, Z.; Liu, Y.-P. Polymorphic Transition of Pre-Oriented Polybutene-1 under Tensile Deformation: In Situ FTIR Study. *Chinese J. Polym. Sci.* **2020**, *38* (8), 888–897. https://doi.org/10.1007/s10118-020-2409-7.

[12] Sängerlaub, S.; Reichert, K.; Sterr, J.; Rodler, N.; von der Haar, D.; Schreib, I.; Stramm, C.; Gruner, A.; Voigt, J.; Raddatz, H.; et al. Identification of Polybutene-1 (PB-1) in Easy Peel Polymer Structures. *Polym. Test.* **2018**, *65* (September 2017), 142–149. https://doi.org/10.1016/j.polymertesting.2017.11.007.

[13] Su, F.; Yang, X.; Dong, B.; Zhao, J.; Lv, F.; Ji, Y.; Liu, C.; Li, L. Investigation on Phase Transition from Flow-Induced Oriented Form II to I in Isotactic Polybutene-1 with in-Situ Microbeam X-Ray Diffraction Technique. *Polymer (Guildf.)* **2019**, *179*, 121719. https://doi.org/10.1016/j.polymer.2019.121719.

[14] Gulturk, E.; Guden, M. Thermal and Acid Treatment of Diatom Frustules. *J. Achiev. Mater. Manuf. Eng.* **2011**, *46* (2), 196–203.

[15] Lamamra, A.; Neguritsa, D. L.; Bedr, S.; Reka, A. A. Determination and Quality Classification of Rock Mass of the Diatomite Mine, Algeria. *News of Ural State Mining Univ.* **2021**, *1* (61), 17–24. https://doi.org/10.21440/2307-2091-2021-1-17-24.

[16] Sever, K.; Atagur, M.; Altay, L.; Seki, Y.; Uysalman, T.; Sen, I.; Kaya, N.; Guven, A.; Sarikanat, M. Effect of Diatomite Weight Fraction on Morphology, Thermal, and Physical Properties of Diatomite Filled High Density Polyethylene Composites. *Acta Phys. Pol. A* **2018**, *134* (1), 281–284. https://doi.org/10.12693/APhysPolA.134.281.

[17] Wu, G.; Ma, S.; Bai, Y.; Zhang, H. The Surface Modification of Diatomite, Thermal, and Mechanical Properties of Poly(Vinyl Chloride)/Diatomite Composites. *J. Vinyl Addit. Technol.* **2019**, *25*, E39–E47. https://doi.org/10.1002/vnl.21664.

[18] Zhao, Y.; Du, M.; Zhang, K. X.; Gao, L. Effect of Modified Diatomite on Crystallinity and Mechanical Properties of Polypropylene. *Mater. Sci. Forum* **2018**, *913*, 551–557. https://doi.org/10.4028/www.scientific.net/MSF.913.551.

[19] Ivanov, S. É.; Belyakov, A. V. Diatomite and Its Applications. *Glass Ceram.* **2008**, *65* (1–2), 48–51. https://doi.org/10.1007/s10717-008-9005-6.

[20] Aguero, A.; Quiles-Carrillo, L.; Jorda-Vilaplana, A.; Fenollar, O.; Montanes, N. Effect of Different Compatibilizers on Environmentally Friendly Composites from Poly(Lactic Acid) and Diatomaceous Earth. *Polym. Int.* **2019**, *68* (5), 893–903. https://doi.org/10.1002/pi.5779.

[21] Wang, K. Y.; Sun, Q. J.; Liu, Y.; Lu, J. Thermal Behavior, Mechanical Property and Microstructure of Low-Density Polyethylene Filled by Diatomite. *Appl. Mech. Mater.* **2014**, *633–634*, 413–416. https://doi.org/10.4028/www.scientific.net/AMM.633-634.413.

[22] Zhan, F.; Chen, N. C.; Zhang, X. H.; Huang, B.; Wu, Z. N.; Zhu, Q. Abrasion Properties and Thermal Stabilities of Poly(Vinylchloride)/Diatomite Composites. *Adv. Mater. Res.* **2014**, *833*, 317–321. https://doi.org/10.4028/www.scientific.net/AMR.833.317.

Chapter I. LITERATURE REVIEW ON POLYOLEFINS, COMPOSITE MATERIALS AND PHYSICAL AND CHEMICAL MODIFICATION TECHNIQUES.

CHAPTER I. LITERATURE REVIEW ON POLYOLEFINS, COMPOSITE MATERIALS AND PHYSICAL AND CHEMICAL MODIFICATION TECHNIQUES

I.1. Polyolefins

A polyolefin is a polymer produced from an olefin or alkene as a monomer. By definition, an olefin or alkene is unsaturated chemical molecule containing at least one carbon to carbon double bond as can been from **Fig I.1**. From recent statistics, the annual production of polyolefins was estimated to represent about 63% of the total polymer production worldwide, reaching nearly 28 Tons for LDPE, 43 Tons HDPE and 80 Tons of PP in 2020 [1]. Polyolefins are composed mainly by three types of polymers: Polyethylene, polypropylene and polybutene-1 as illustrated in **Fig I.2.**

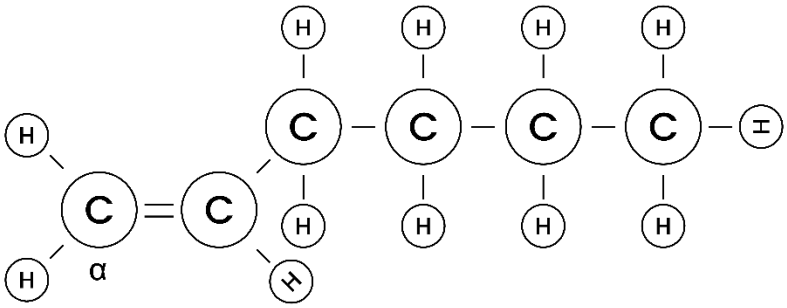

Fig I.1. Olefin structure.

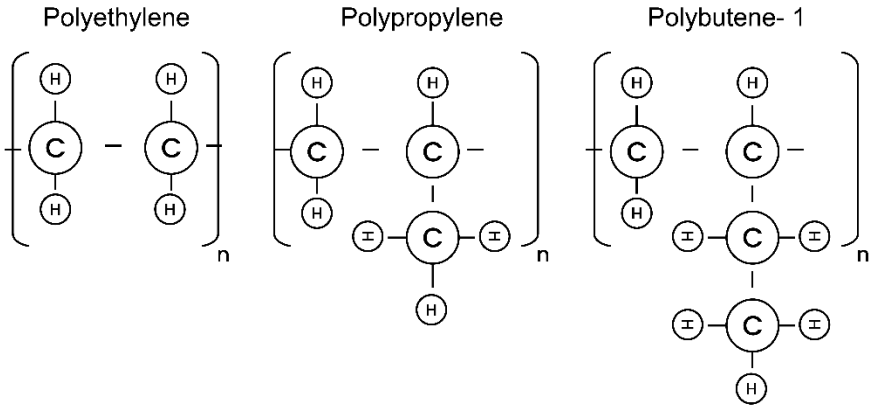

Fig I.2. Polyolefins polymers.

I.1.1. Polyethylene (PE)

Polyethylene was first discovered in the beginning of 1933 by accident, where two chemists, Eric Fawcett and Reginald Gibson were trying to condense ethylene with benzaldehyde at high pressure and temperature (142 MPa and 170°C), which resulted in the apparition of small residue that was concluded later to be polyethylene. After this discovery, researchers from the Imperial Chemical Industries (ICI) continue to work on the polymerization of polyethylene where they finally succeeded in producing larger amounts in the late of 1935 and ultimately commercialized in 1939 into what is known these days Low-Density Polyethylene (LDPE) [1].

I.1.1.1. Classification and types of PE

Considering it density range, polyethylene was classified by the society of the plastic industry (SPI) as follow:

1. **Very-low density polyethylene (VLDPE)**: Also known as ultra-low-density PE (ULDPE), produced by Ziegler-Natta catalysts using α-olefin comonomers, having a density from 0.855 to 0.915 g/cc. selected grades of VLDPE produced with single-site catalysts are known as polyolefin plastomers (POP) and polyolefin elastomers (POE), both displaying a thermoplastic and rubbery characteristic at the same time;
2. **Low-density polyethylene (LDPE):** produced only by free radical polymerization of ethylene induced by organic peroxide or reagents readily decomposes into free radicals. LDPE is the most easily processed of major types of PE and is often blended with LLDPE and HDPE to improve their processability. Due to the high branching degree, it contains high amorphous content resulting in an outstanding clarity in films for food packaging industry;
3. **Linear low-density polyethylene (LLDPE):** produced by copolymerization of ethylene with α-olefin using Ziegler-Natta, supported chromium or single site catalysts and cannot be polymerized by free radical polymerization resulting in a density of 0.915-0.930 g/cc. butene-1, hexene-1 and octene-1 are the most common comonomers resulting in LLDPE with short chain branches of ethyl, n-butyl and n-hexyl groups respectively. The mechanical properties of LLDPE are more superior to those of LDPE, but due to its low amorphous content, it tends to produce a less clear films compared to LDPE based films;
4. **Medium-density high-density polyethylene (MDPE or MDHDPE):** produced by copolymerization of ethylene with α-olefin using Ziegler-Natta, supported chromium or single site catalysts. MDPE has a linear structure similarly to LLDPE with the only difference

in the low content of comonomers. With a density 0.93-0.94 g/cc, MDPE is used in geomembrane and pipes applications;

5. **High molecular weight HDPE (HMWHDPE):** produced by Ziegler-Natta or chromium supported catalysts and it's characterized by its high molecular weight (200000-500000 amu) and a density of 0.94-0.96 g/cc. used in pipes and automotive fuel tanks;
6. **Ultra-high molecular weight polyethylene (UHMWPE):** produced by Ziegler-Natta catalysts and it's characterized a very high molecular weight (3000000-7000000amu) and a density similar to HDPE of 0.94 g/cc due to the crystalline defects and lamellar effects caused by the enormously long polymer chains, resulting in an excellent impact strength and abrasion resistance. UHMWPE is considered to be tough to process on standard machines but could be molded via compression molding process into a variety of products, such as prosthetic devices like artificial hips or extruded into a tough fiber used in the manufacturing of bullet proof vests;

I.1.1.2. High-Density Polyethylene (HDPE)

HDPE is composed mainly by carbons and hydrogen molecules, polymerized from an ethylene monomer using a Ziegler-Natta catalyst. The degree of branching is much lower in the case of HDPE as in LDPE as shown in **Fig I.3** [2] , which results in higher degree of crystallinity (50-90%), higher density (0.94-0.96 g/cc) and also a higher melting temperature (130-138°C), thus leading a much superior properties such as, the tensile strength, stiffness, chemical resistance, ease of processing, chemical and water resistance. It also known for its recyclability, low cost, flexibility, toughness, along with many other features [3, 4].

However, accompanying these advantages features, it also lacks the resistance to stress cracking, low temperature brittleness, high mold shrinkage [5], low melting temperature, which restricts its use in high temperature conditions, and non-polarity, hindering its adhesion to metallic or polar surfaces and due to its high crystallinity, it cannot match the clarity of LDPE or LLDPE films. HDPE found its place in many applications, like in potable water pipes, blow molded household packaging and industrial chemicals like bottles for bleach, shampoo, detergent, etc. [1, 6] .

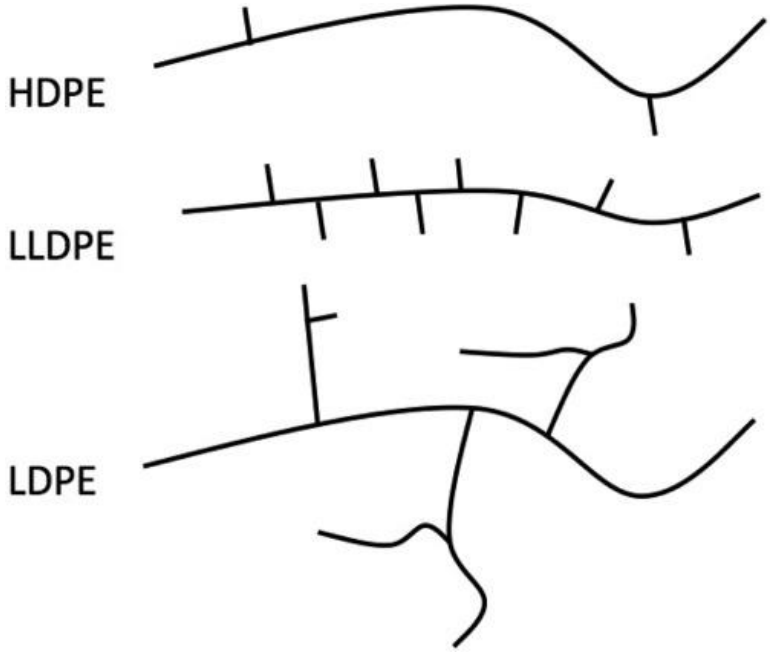

Fig I.3. HDPE, LLDPE and LDPE structures.

I.1.2. Isotactic Polybutene-1 (PB-1)

Polybutene-1 was synthesized for the first time in 1954 [1, 7] right after the year when PP was synthesized for the first time, yet it was not manufactured in large scales only after 10 years later. Depending on the position of the carbon double bond in the monomer, polybutene could appear in linear form if the double bond lies between the first and second carbon atoms of the monomer (butene-1), resulting in what is called polybutene-1 (PB-1), which a chemical structure similar to PP, as shown in **Fig I.4**. Whereas, the branched monomer results in a totally different polymer called isobutylene (PIB). PB-1 is produced from the polymerization of butene-1 with Ziegler-Nata catalysts resulting in a more linear, high molecular weight, isotactic and semi-crystalline structure [1]. it's known to be a polymorphic polymer, characterized by four distinctive crystalline forms, called form I, I', II and III, with form I/I' both having a hexagonal unit cell structure, while form II and III having a tetragonal and orthorhombic structures respectively. The formation of each crystal form is dependent on the preparation condition and the manner of how they were processed. During cooling from the melt, PB-1 crystallizes rapidly into the metastable form II under ambient conditions. In a time, duration of several days up to a couple of weeks, PB-1 gradually and spontaneously transform into a more thermodynamically stable form I, under which it possesses the most superior and favorable properties and higher melting point [8–14]. Beside the outstanding characteristics offered from the Form I crystalline structure, yet it still shows some drawbacks, like the long time consuming during the transformation and the outcomes of such transitioning process, like the shrinkage that results in defects in the final product [13, 15, 16].

Form I' has a similar unit cell structure as Form I, forming from solution precipitation or under applied pressure, yet it has a different melting point. Form III on the other hand, is the least perfect crystal modification, resulting from dried solutions [13].

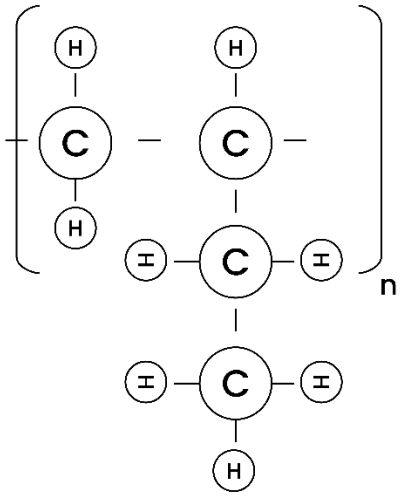

Fig I.4. Polybutene-1 Structure.

Characteristics and application fields

With different crystallinity degree, differs its physical and mechanical properties, thus its application field. Like the other polyolefins, PB-1 offers a good chemical resistance, endurance to environmental stress cracking and more particularly, excellent creep properties even at elevated temperatures, good flexibility and elasticity, abrasion resistance and high puncture resistance in film applications [11, 17–21], which makes it a good choice for high durability requiring products, like pressurized tanks, hot and cold water plumbing pipes, especially pressurized pipes that are exposed to chlorinated water due to their long term performance in comparison to regular polyolefins pipes [22] and other technical products, such as easy-to-peel packaging for cereals, coffee powder, meat and frozen foods storage and hot melt adhesives [12, 14, 17, 19]. Since the crystalline form I is the most favorable modification in term of physical and mechanical properties, transformation from Form II to Form I was the main focus of the researchers. X. yang et al [17], investigated the phase transition of iPB-1 from form II to I induced by stretching under different tensile conditions at atmospheric temperatures, where it was found that when stretched to strains beyond yielding point, iPB-1 shows an accelerated phase transition rate. Other orientation and mechanical approaches were utilized to accelerate the transformation rate [16, 20]. Blending polymers with iPB-1, was another method for accelerating the phase II to I transformation rate. A. Liang et al [15], have found that the addition of iPP in small ratios into iPB-1 enhance greatly the transformation rate from Form II to Form I. Lou et

al [9], found that grafting polyethylene glycol (PEG) into iPB-1 chains enhanced the crystallization behavior and significantly accelerated the phase II to I transition. M. Kaszonyiova et al [10], found that exposing iPB-1 to solvents such as gasoline, toluene, xylene, benzene trichloromethane have a positive influence on the transitioning rate from Form II to I. Compounding iPB-1 with additives is another potential mean of accelerating the transformation rate. Nanofillers, like nanosilica and nano layered silicate were found to possess a noticeable accelerating effect on the phase II to I transformation [8, 23]. On the other hand, the addition of other additives, such as mica, sodium chloride, graphite and talc were found to have a retarding effect on the crystallization rate [16].

I.2. Composite materials

Blending binary, tertiary or even more polymers together is a cost-effective way to combine the performances of the component polymers or at least to get the properties of one them in comparison to polymerization or copolymerization method [24]. A very good example is mixing an elastomer with a rigid polymer in order to balance between the toughness and stiffness. Reinforcing polymeric materials with different sized organic or inorganic substances is very common technique to alter its properties, its flow behavior, reducing the cost and even improve the mechanical, thermal and barrier properties if the filler particles are well dispersed and adhered to the polymer chains [4, 24]. On the other hand, the incorporation of nano-sized fillers into polymeric matrix to produce what it is known as a nanocomposite, was found to be far more interesting in term of the yielded properties even at small ratios of the filler. Multi-walled carbon nanotubes (MWCNT) are one example of the nanofillers used in polymeric materials, as its incorporation with HDPE showed a great enhancement in the wear resistance properties [25]. The incorporation of conductive fillers into polymer matrix, such as carbon black (CB), carbon nanotubes (CNT) or graphene nanoplatelet (GNP) results in increment of both the electrical and thermal conductivity, which turn out to be useful in the electronic industry [4].

I.2.1. Diatomaceous earth-based composites

I.2.1.1. Diatomaceous earth

Diatomite, also known as Diatomaceous earth or kieselguhr [26, 27], is a sedimentary rock formed by fossilized diatom shells (or frustules). The latter are mainly composed by hydrated amorphous silica (SiO_2, nH_2O) in the order of few tens of nanometers, along with other organic impurities, clay and metal oxides. It could be found in different colors depending on its composition, from light colored

white, yellowish up to a darker brownish color which is caused by the organic impurities present on its surface and within its pores [28].

Owing to its outstanding features, such the light weight, low density, chemical resistance, high surface area, thermal resistance and high porosity, it gained a great popularity in many industrial fields, from the food sector, cosmetics, pharmaceutical, petroleum, chemical and also in the coating, plastic and rubber industries [5]. The porous structure and the high surface area along with its good chemical resistance, makes it a great filtration media for a different type of organic and inorganic materials [29, 30] and since it possesses a nanometer pore [28] and its mainly formed by silica, it was seen as a good candidate as a nano filler for polymeric materials [31, 32].

I.2.1.2. Study cases

Several studies were conducted on the Diatomaceous earth-based composites. Zhan, F et al, [33] studied the effect of the pristine Diatomaceous earth content on the thermal and abrasion properties of the PVC/Diatomaceous earth composites, where a noticeable increase in thermal resistance and the abrasion properties were observed by the increase of the Diatomaceous earth content (from 0 to 80 phr), while both the tensile strength and the impact resistance decreased. In another study, Wu, G et al, [29] investigated the effect of the surface treated Diatomaceous earth on the thermal and mechanical properties of PVC/Diatomaceous earth composites, where the Diatomaceous earth was first cleaned with hydrochloric acid in order to remove the adhered impurities, and the metal oxides in particular on both the surface and within the pores, and then treated with silane coupling agent to improve the interfacial interaction with the polymeric matrix. It was found that both the impact strength and the thermal stability of the composites decreased at higher Diatomaceous earth concentration due to agglomeration of the latter. Wang, K et al [32] investigated the thermal, mechanical and morphological properties of LDPE filled with titanate coupling agent surface modified Diatomaceous earth. It was observed that the Diatomaceous earth affected the crystallization of the LDPE, where it was seen to forward the crystallization and reduced its rate, while the titanate coupling agent improved the dispersion of the filler in the polymer matrix as can be seen from the SEM micrographs. Sever, K et al [5], studied the effect of Diatomaceous earth content (5, 10, 15 and 20 %) on HDPE properties, where no considerable changes were seen on the tensile and flexural strengths due to the poor interactions between the filler particles and the HDPE matrix as revealed from the SEM micrographs, whereas a decrease by 7% in the thermal endurance and an increase in the stiffness were observed by the increase of the Diatomaceous earth concentration. PP/Diatomaceous earth composites properties were investigated after the

Diatomaceous earth were surface modified by four types of coupling agents [30]. PLA/Diatomaceous earth bio-composites properties were investigated in the presence of malenized linseed oil (MLO) as a compatibilizer and a bio-plasticizer [31], where the Diatomaceous earth addition seemed to induce a more embrittlement behavior in the PLA matrix (Increased the stiffness) due to the stress concentration phenomena, whereas the MLO induced a better dispersion of the filler particles in the matrix as shown from SEM micrographs. Diatomaceous earth was also used as a reinforcement filler for rubber materials in replacement to carbon black and silica. In a study performed by Wu, W et al, [34] Where they used a silane (Si69) treated diatomaceous earth after purification with sulfuric acid as a reinforcement filler for several types of synthetic rubbers, and it was found to be most efficient in the case of florin rubbers, EPDM and acrylate rubbers.

Beside acting as a filler in the polymeric composites, Diatomaceous earth was also used as an additive. In recent advancement in the packaging industry, a new type of packaging system known as active packaging is now being used, where some active components such as antioxidants and antimicrobials are imbedded into the polymer matrix or encapsulated into different particles/microcapsules to control their release during the storage time of food. Clays such as Montmorillonite (MMT) and Halosite nanotube (HWT) were used as carrier for these types of active agents. Recently, Diatomaceous earth was also proven to be a good candidate as a carrier for active agents due its high porosity and chemical resistance [31].

Diatomaceous earth was also used as processing aid in combination with polyethylene glycol (PEG) [35], where it showed a better effect on reducing the viscosity of the mLLDPE in comparison to the PEG alone. In another study, Shih, Y et al, [36] have successfully developed an eco-friendly halogen free flame retarding system based on Diatomaceous earth along with ammonium polyphosphate (APP) and expanded graphite (EG).

I.3. Physical and Chemical modification

Polymer crosslinking reaction is a very common technique used to alter its physical and mechanical characteristics in order to broaden its application range, such as the enhancement of its high temperature performance, superior mechanical strength, high impact resistance, low thermal expansion, resistance to solvents and chemicals, and so many other desired features [37]. The crosslinking reaction can be achieved via a physical method using ionizing radiation from γ-rays emitted by a radioactive isotope like cobalt 60 (^{60}Co), electron beams, or X-ray radiation [38], chemically using silanes [39] or organic peroxides [40]. Chemical crosslinking using organic peroxides is the most common method used in recent years, which is based on the formation of macro-radicals

resulting from the extraction of a hydrogen molecule from the polymer backbone induced by the attack from the oxy-radicals that are formed by the decomposition of the organic peroxide at high temperatures, resulting in an interconnected network between the polymeric chains [41]. Besides the aforementioned advantages offered by the crosslinking reaction, one of the biggest challenges resulting from this kind of reaction is the high brittleness and non-recyclability of the formed product, behaving more as thermosets than elastomers.

Reversible Crosslinking Reaction (RXR)

Since recyclability is a desired feature in almost all types of materials and in plastics in particular for a cleaner and less pollutant environment, the harmful impact of their disposal both in the sea and in landfills. For this reason, many researchers are now seeking to develop new recyclable cross-linked polymers. Bouhelal et al. [42–44] developed an original reversibly crosslinking reaction (RXR) based on mixing the polymer with an accelerator, sulfur, and organic peroxide in the melt state via the reactive-extrusion process, resulting in a recyclable crosslinked polymer with outstanding properties. Similarly to the regular peroxide-induced crosslinking reaction, macroradicals are formed by an attack from the oxy-radicals on the polymer chains, with the only difference residing in the formation of sulfur-based compounds (sulfur atoms, polysulfide, or a cyclic sulfur compound) bridges between the macroradicals instead of interlocking with themselves [45] .H. Saci et al. [41] investigated the crosslinking of low-density polyethylene (LDPE) with the new RXR technique using three different systems: peroxide, peroxide/accelerator, and peroxide/accelerator/sulfur. The crosslinking reactions of three systems were studied by dynamic rheological analysis (DRA) using a Brabender plasticorder. An enhancement in thermal stability was recorded from the TGA test, which may be attributed to the sulfur presence. On the other hand, the recyclability of the blends was monitored by a simple compression molding test, where it was clearly seen that the peroxide-crosslinked blends tend to decompose when tried to be remolded, while the other two systems with peroxide/accelerator and peroxide/accelerator/sulfur can be remolded again and again when compression molded. S. Bouhelal et al [46]. have successfully prepared a reversibly crosslinked isotactic polypropylene (iPP) using the RXR technique, even though that iPP is considered a non-crosslinkable polymer due to the beta-scission degradation reaction that predominates in the crosslinking reaction as explained from the **Fig I.5**. The crosslinking reaction resulted in a ductile iPP with a great impact resistance improvement of almost seven times that of the neat iPP.

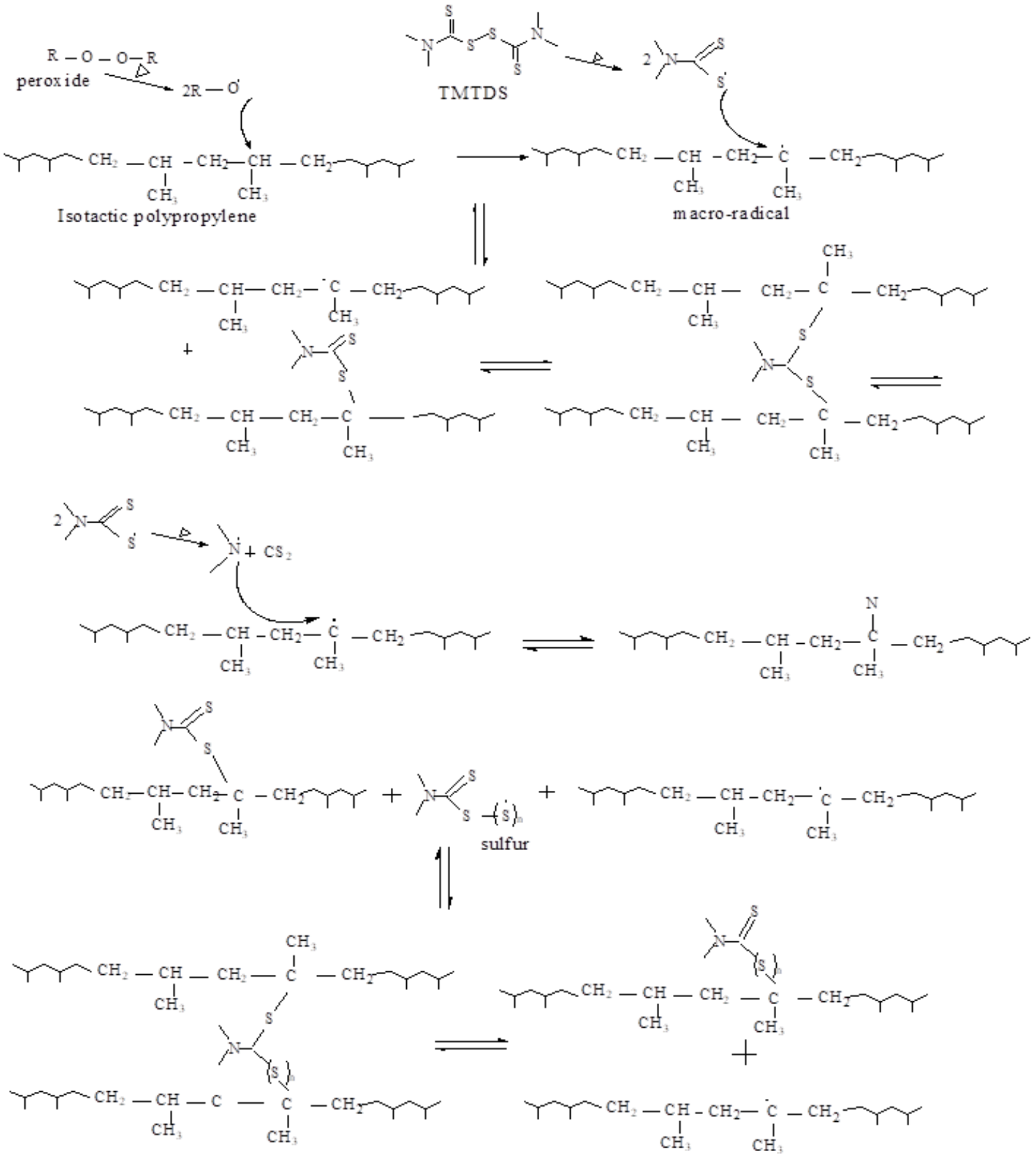

Fig I.5. Reversible crosslinking reaction of iPP.

References

[1] Kutz, M. *Applied Plastics Engineering Handbook: Processing, Materials, and Applications*, 2nd ed.; William Andrew: Amsterdam, Netherlands. https://doi.org/10.1016/C2014-0-04118-4.

[2] Ragaert, K.; Delva, L.; Van Damme, N.; Kuzmanovic, M.; Hubo, S.; Cardon, L. Microstructural Foundations of the Strength and Resilience of LLDPE Artificial Turf Yarn. *J. Appl. Polym. Sci.* 2016, *44080*. https://doi.org/10.1002/app.44080.

[3] Ronca, S. Polyethylene. In *Brydson's Plastics Materials*; Elsevier, 2017; pp 247–278. https://doi.org/10.1016/B978-0-323-35824-8.00010-4.

[4] Li, Y.; Li, D.; Cheng, H.; Han, C.; Xiao, L. Morphology and Physical Properties of Composites Based on High-Density Polyethylene/Propylene-Ethylene Random Copolymers Blends and Carbon Black. *Polym. Test.* 2023, *123*, 108050. https://doi.org/10.1016/j.polymertesting.2023.108050.

[5] Sever, K.; Atagur, M.; Altay, L.; Seki, Y.; Uysalman, T.; Sen, I.; Kaya, N.; Guven, A.; Sarikanat, M. Effect of Diatomite Weight Fraction on Morphology, Thermal and Physical Properties of Diatomite Filled High Density Polyethylene Composites. *Acta Phys. Pol. A* 2018, *134*(1), 281–284. https://doi.org/10.12693/APhysPolA.134.281.

[6] Malpass, D. *Introduction to Industrial Polyethylene: Properties, Catalysts, and Processes*; Wiley-Scrivener: Hoboken, NJ, 2020.

[7] Abedi, S.; Sharifi-Sanjani, N. Preparation of High Isotactic Polybutene-1. *J. Appl. Polym. Sci.* 2000, *78*(14), 2533–2539. https://doi.org/10.1002/1097-4628(20001227)78:14<2533::AID-APP140>3.0.CO;2-U.

[8] Kulkarni, D.; Jyoti, P. J. Effect of Nano Silica on Phase Transformation from Form-II to Form-I of Polybutene-1. *Int. Res. J. Eng. Technol.* 2020, *07*(11), 4.

[9] Lou, Y.-H.; Li, W.; Qv, C.-J.; Ma, Z. Enhanced Phase Transition in Poly(Ethylene Glycol) Grafted Butene-1 Copolymers. *Chin. J. Polym. Sci.* 2023, *41*(3), 414–421. https://doi.org/10.1007/s10118-022-2850-x.

[10] Kaszonyiova, M.; Rybnikar, F. Influence of the Environment on the Phase II-I Transformation of Isotactic Polybutene-1. *J. Macromol. Sci., Part B: Phys.* 2019, *58*(2), 248–262. https://doi.org/10.1080/00222348.2019.1574424.

[11] Andena, L.; Rink, M.; Frassine, R.; Corrieri, R. A Fracture Mechanics Approach for the Prediction of the Failure Time of Polybutene Pipes. *Eng. Fract. Mech.* 2009, *76*(18), 2666–2677. https://doi.org/10.1016/j.engfracmech.2009.10.002.

[12] Su, F.; Yang, X.; Dong, B.; Zhao, J.; Lv, F.; Ji, Y.; Liu, C.; Li, L. Investigation on Phase Transition from Flow-Induced Oriented Form II to I in Isotactic Polybutene-1 with In-Situ Microbeam X-Ray Diffraction Technique. *Polymer (Guildf.)* 2019, *179*, 121719. https://doi.org/10.1016/j.polymer.2019.121719.

[13] Hu, D.; Li, W.; Wu, K.; Cui, L.; Xu, Z.; Zhao, L. Utilization of Supercritical CO2 for Controlling the Crystal Phase Transition and Cell Morphology of Isotactic Polybutene-1 Foams. *J. CO2 Util.* 2022, *66*, 102265. https://doi.org/10.1016/j.jcou.2022.102265.

[14] Wei, X.; Qu, Y.; Jiang, H.; Huang, Z.-X.; Qu, J.-P. Melt-State Dynamic Pressure Engineered Polybutene-1 with Form I Crystals. *Polymer (Guildf.)* 2022, *256*, 125185. https://doi.org/10.1016/j.polymer.2022.125185.

[15] Liang, A.; Li, J.; Jiang, S. Role of Amorphous Phase in II-I Transition of IPB-1/IPP Blends. *Polymer (Guildf.)* 2024, *296*, 126818. https://doi.org/10.1016/j.polymer.2024.126818.

[16] Kaszonyiova, M.; Rybnikar, F.; Geil, P. H. Phase Transitions in Isotactic Polybutene-1. *J. Macromol. Sci., Part B: Phys.* 2019, *58*(2), 263–274. https://doi.org/10.1080/00222348.2019.1578521.

[17] Afrifah, K. A.; Hickok, R. A.; Matuana, L. M. Polybutene as a Matrix for Wood Plastic Composites. *Compos. Sci. Technol.* 2010, *70*(1), 167–172. https://doi.org/10.1016/j.compscitech.2009.09.019.

[18] Schössig, M.; Grellmann, W.; Mecklenburg, T. Characterization of the Fracture Behavior of Glass Fiber Reinforced Thermoplastics Based on PP, PE-HD, and PB-1. *J. Appl. Polym. Sci.* 2010, *115*(4), 2093–2102. https://doi.org/10.1002/app.31271.

[19] Yang, X.; Dong, B.; Shang, Y.; Ji, Y.; Su, F.; Shao, C.; Wang, Y.; Liu, C.; Shen, C. Investigation on the Phase Transition from Form II to Form I in IPB-1 after Pre-Stretching. *Polymer (Guildf.)* 2020, *194*, 122385. https://doi.org/10.1016/j.polymer.2020.122385.

[20] Zhang, Z.; Chen, X.; Zhang, C.; Liu, C.-T.; Wang, Z.; Liu, Y.-P. Polymorphic Transition of Pre-Oriented Polybutene-1 under Tensile Deformation: In Situ FTIR Study. *Chin. J. Polym. Sci.* 2020, *38*(8), 888–897. https://doi.org/10.1007/s10118-020-2409-7.

[21] Lundbäck, M.; Hassinen, J.; Andersson, U.; Fujiwara, T.; Gedde, U. W. Polybutene-1 Pipes Exposed to Pressurized Chlorinated Water: Lifetime and Antioxidant Consumption. *Polymer Degradation and Stability*, 2006, *91*(4), 842–847. https://doi.org/10.1016/j.polymdegradstab.2005.06.015.

[22] Sängerlaub, S.; Reichert, K.; Sterr, J.; Rodler, N.; von der Haar, D.; Schreib, I.; Stramm, C.; Gruner, A.; Voigt, J.; Raddatz, H.; et al. Identification of Polybutene-1 (PB-1) in Easy Peel Polymer Structures. *Polymer Testing*, 2018, *65*, 142–149. https://doi.org/10.1016/j.polymertesting.2017.11.007.

[23] Wanjale, S. D.; Jog, J. P. Poly (1-Butene)/Clay Nanocomposites: A Crystallization Study. *Journal of Macromolecular Science, Part B: Physics*, 2003, *42*(6), 1141–1152. https://doi.org/10.1081/MB-120024810.

[24] Zhang, Q.; Khan, M. U.; Lin, X.; Cai, H.; Lei, H. Temperature Varied Biochar as a Reinforcing Filler for High-Density Polyethylene Composites. *Composites Part B: Engineering*, 2019, *175*, 107151. https://doi.org/10.1016/j.compositesb.2019.107151.

[25] Dabees, S.; Tirth, V.; Mohamed, A.; Kamel, B. M. Wear Performance and Mechanical Properties of MWCNT/HDPE Nanocomposites for Gearing Applications. *Journal of Materials Research and Technology*, 2021, *12*, 2476–2488. https://doi.org/10.1016/j.jmrt.2020.09.129.

[26] Gulturk, E.; Guden, M. Thermal and Acid Treatment of Diatom Frustules. *Journal of Achievements in Materials and Manufacturing Engineering*, 2011, *46*(2), 196–203.

[27] Lamamra, A.; Neguritsa, D. L.; Bedr, S.; Reka, A. A. Determination and Quality Classification of Rock Mass of the Diatomite Mine, Algeria. *News of the Ural State Mining University*, 2021, *1*(61), 17–24. https://doi.org/10.21440/2307-2091-2021-1-17-24.

[28] Ivanov, S. É.; Belyakov, A. V. Diatomite and Its Applications. *Glass and Ceramics*, 2008, *65*(1–2), 48–51. https://doi.org/10.1007/s10717-008-9005-6.

[29] Wu, G.; Ma, S.; Bai, Y.; Zhang, H. The Surface Modification of Diatomite, Thermal, and Mechanical Properties of Poly(Vinyl Chloride)/Diatomite Composites. *Journal of Vinyl and Additive Technology*, 2019, *25*, E39–E47. https://doi.org/10.1002/vnl.21664.

[30] Zhao, Y.; Du, M.; Zhang, K. X.; Gao, L. Effect of Modified Diatomite on Crystallinity and Mechanical Properties of Polypropylene. *Materials Science Forum*, 2018, *913*, 551–557. https://doi.org/10.4028/www.scientific.net/MSF.913.551.

[31] Aguero, A.; Quiles-Carrillo, L.; Jorda-Vilaplana, A.; Fenollar, O.; Montanes, N. Effect of Different Compatibilizers on Environmentally Friendly Composites from Poly(Lactic Acid) and Diatomaceous Earth. *Polymer International*, 2019, *68*(5), 893–903. https://doi.org/10.1002/pi.5779.

[32] Wang, K. Y.; Sun, Q. J.; Liu, Y.; Lu, J. Thermal Behavior, Mechanical Property and Microstructure of Low-Density Polyethylene Filled by Diatomite. *Applied Mechanics and Materials*, 2014, *633–634*, 413–416. https://doi.org/10.4028/www.scientific.net/AMM.633-634.413.

[33] Zhan, F.; Chen, N. C.; Zhang, X. H.; Huang, B.; Wu, Z. N.; Zhu, Q. Abrasion Properties and Thermal Stabilities of Poly(Vinylchloride)/Diatomite Composites. *Advanced Materials Research*, 2014, *833*, 317–321. https://doi.org/10.4028/www.scientific.net/AMR.833.317.

[34] Wu, W. L.; Chen, Z. Modified-Diatomite Reinforced Rubbers. *Materials Letters*, 2017, *209*, 159–162. https://doi.org/10.1016/j.matlet.2017.07.133.

[35] Liu, X.; Xie, M.; Li, H. Effect of Inorganic Fillers in Binary Processing Aids on the Rheology of a Metallocene Linear Low-Density Polyethylene. *Journal of Applied Polymer Science*, 2005, *96*(5), 1824–1829. https://doi.org/10.1002/app.20968.

[36] Shih, Y. F.; Tsai, W. L.; Kotharangannagari, V. K. Development of Eco-Friendly Flame-Retarded High Density Polyethylene Composites. In *Key Engineering Materials*; Trans Tech Publications Ltd, 2020; Vol. 847, pp 55–60. https://doi.org/10.4028/www.scientific.net/KEM.847.55.

[37] Lepage, M. L.; Simhadri, C.; Liu, C.; Takaffoli, M.; Bi, L.; Crawford, B.; Milani, A. S.; Wulff, J. E. A Broadly Applicable Cross-Linker for Aliphatic Polymers Containing C–H Bonds. *Science*, 2019, *366*(6467), 875–878. https://doi.org/10.1126/science.aay6230.

[38] Al-Ghamdi, H.; Farah, K.; Almuqrin, A.; Hosni, F. FTIR Study of Gamma and Electron Irradiated High-Density Polyethylene for High Dose Measurements. *Nuclear Engineering and Technology*, 2022, *54*(1), 255–261. https://doi.org/10.1016/j.net.2021.07.023.

[39] Dana, M.; Zohuri, G. H.; Asadi, S.; Salahi, H. A New Approach for Silane Curing Polyolefin Elastomer/Linear Low Density Polyethylene Blends by Monosil and Sioplas Processes. *Journal of Macromolecular Science, Part A*, 2020, *57*(1), 9–16. https://doi.org/10.1080/10601325.2019.1571867.

[40] Song, R. Manufacturing, Structure, and Properties of Crosslinked Polyethylene Induced by Peroxides. *Department of Materials Science and Engineering, University of Washington, Seattle, WA 98185, USA*, 2020. https://doi.org/10.6069/902T-QF03.

[41] Saci, H.; Bouhelal, S.; Bouzarafa, B.; López, D.; Fernández-García, M. Reversible Crosslinked Low Density Polyethylenes: Structure and Thermal Properties. *Journal of Polymer Research*, 2016, *23*(4), 68. https://doi.org/10.1007/s10965-016-0965-x.

[42] Bouhelal, S. Recyclable Isotactic Polypropylene. *US Patent 7,524.901 B1*, 2009.

[43] Bouhelal, S.; Cagiao, M. E.; Benachour, D.; Djellouli, B.; Rong, L.; Hsiao, B. S.; Baltá-Calleja, F. J. SAXS Study Applied to Reversibly Crosslinked Isotactic Polypropylene/Clay Nanocomposites. *Journal of Applied Polymer Science*, 2010, n/a-n/a. https://doi.org/10.1002/app.32241.

[44] Bouhelal, S.; Cagiao, M. E.; Khellaf, S.; Benachour, D.; Baltá Calleja, F. J.; Calleja, F. J. B. Structure and Properties of New Reversibly Crosslinked IPP/LDPE Blends. *Journal of Applied Polymer Science*, 2008, *109*(2), 795–804. https://doi.org/10.1002/app.28194.

[45] Bouhelal, S. Article Formed from Cross-Linking Isotactic Polymers in the Presence of Peroxide. *US Patent 7,309,744 B2*, 2007.

[46] Bouhelal, S.; Cagiao, M. E.; Benachour, D.; Calleja, F. J. B.; Baltá Calleja, F. J.; Calleja, F. J. B. Structure Modification of Isotactic Polypropylene through Chemical Crosslinking: Toughening Mechanism. *Journal of Applied Polymer Science*, 2007, *103*(5), 2968–2976. https://doi.org/10.1002/app.25406.

CHAPTER II. MATERIALS AND METHODOLOGY

CHAPTER II. MATERIALS AND METHODOLOGY

This chapter describes all the materials used in our study and a summary of the formulation components. There is also an in-depth explanation of the methods used to characterize the samples, the experimental methodology, melt mixing, and compounding steps.

II.1. Materials

II.1.1. High Density Polyethylene (HDPE)

Extrusion grade HDPE from SABIC (Saudi Arabia) with a melt flow index (MFI) of 0.06 g/10 min (230 °C, 2.16 kg load).

II.1.2. Isotactic Polybutene-1 (PB-1)

Isotactic Polybutene-1 (PB-1) was purchased from BASELL (Saudi Arabia), having a low melt flow index (MFI) of 0.37 g/10 min (230 °C, 2.16 kg load).

II.1.3. Dicumyl peroxide (DCP)

The radical initiator, Dicumyl peroxide (DCP), with 96 wt % activity was supplied by NORAX (Germany).

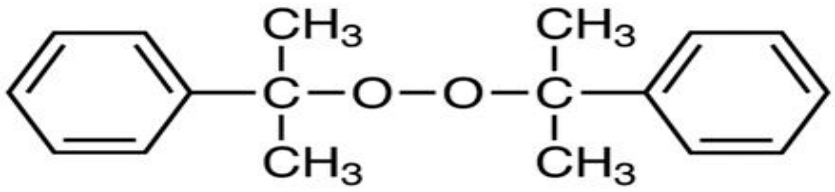

Fig II.1. Dicumyl peroxide molecular structure.

II.1.4. Sulfur (S8)

High purity industrial grade, Sulfur (S8) was supplied by Wuxi Huasbeng Chemical Additives (China).

II.1.5. Tetramethyl Thiuram Disulfide (TMTD)

TMTD accelerator “Super accelerator 501’’ was used, as supplied by Rhone-Poulenc, France.

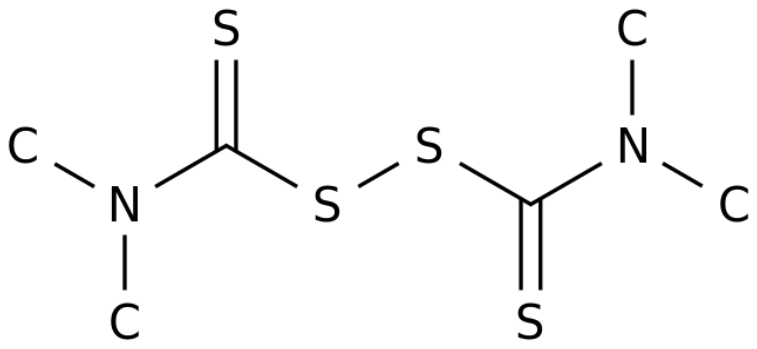

Fig II.2. TMTD molecular structure.

II.1.6. Diatomaceous earth

In form of reddish rock, pristine Diatomaceous earth was sourced from sig (mascara), by National Company of Non-Ferrous Mining Products and Useful Substances (ENOF) Spa in Algeria. Having a Young's modulus E = 0.533 MPa, a surface area of 70.35 m^2/g, a particle median diameter d_{50} = 16 µm, and consist of hydrated amorphous silica (opal), organic matter, metal oxides, clay, and other substances as listed in **Table II.1**.

Table II.1. Chemical composition of pristine diatomaceous earth.

Composition	**SiO_2**	**CaO**	**Al_2O_3**	**Fe_2O_3**	**MgO**	**K_2O**	**Na_2O**	**TiO_2**
Weight %	63	26.9	3.58	1.87	1.91	1.04	0.59	0.28

II.2. Composites preparation

Pristine Diatomaceous earth rocks were first crushed using a laboratory mortar and a pestle, followed by a calcination process at a temperature range exceeding 900 °C for a duration of 4 h, after being gradually heated in an oven at 110 °C for 1 h, and finally sieved using a 20 µm laboratory sieve.

The reactive extrusion process was used for the preparation of the different mixtures in the melt state using a BRABENDER PLASTICORDER at optimal predetermined conditions (mixing speed = 30–50 rpm, t =10 min and a temperature of 190 °C). The mixed batches were then shredded and compression molded by a laboratory hot press at 190°C for a total of 12 minutes (7 min preheating, 5 min molding) into thin films for FTIR and WAXS characterizations and into dumbbell-shaped and rectangular-shaped specimens for the tensile and impact resistance tests, respectively. The remaining impact test specimens were fractured after being immersed in liquid nitrogen for several

minutes and sputter coated with a thin layer of gold for the SEM analysis. The reversibly crosslinking agent (RXR) was prepared elsewhere. The prepared batches are codified like the following:

HDPE-xD and **HDPE-MxD**, where (**x**) refers to the weight fraction of the Diatomaceous earth, (**D**): Diatomaceous earth-filled samples, and (**M**) refers to the modification using the RXR agent as summarized in **Table II.1.**

Table II.2. HDPE microcomposites designation and compositions.

	HDPE wt%	Diatomaceous earth wt%	RXR wt%
HDPE	100	0	0
HDPE-2D	98	2	0
HDPE-4D	96	4	0
HDPE-6D	94	6	0
HDPE-M2D	97.5	2	0.5
HDPE-M4D	95.5	4	0.5
HDPE-M6D	93.5	6	0.5

PB-1/xD and **PB-1/MxD**, where (**x**) refers to the weight fraction of the Diatomaceous earth (**D**): Diatomaceous earth-filled samples, and (**M**) refers to the modification using the RXR agent as summarized in **Table II.3.**

Table II.3. PB-1 microcomposites designation and compositions.

	PB-1 wt%	Diatomaceous earth wt%	RXR wt%
PB-1	100	0	0
PB-1/0.5D	99.5	0.5	0
PB-1/1D	99	1	0
PB-1/2D	98	2	0
PB-1/4D	96	4	0
PB-1/M0.5D	99	0.5	0.5
PB-1/M1D	98.5	1	0.5
PB-1/M2D	97.5	2	0.5
PB-1/M4D	95.5	4	0.5

II.3. Characterization techniques

II.3.1. Diatomaceous earth characterization

II.3.1.1. Particle size distribution

The particle size and particle size distribution of the filler was investigated by a laser scattering particle size distribution analyzer from HORIBA.

II.3.1.2. Fourier transform infrared (FTIR)

Powdered Pristine Diatomaceous earth was analyzed using a Shimadzu LabSolutions IR spectroscopy in wavenumber range of 400-4000 cm^{-1} after being calcined and sieved into a fine powder.

II.3.1.3. Scanning electronic microscopy (SEM)

Neoscope JCM-5000 scanning electron microscope was used to scan the powdered Diatomaceous earth filler at a magnification of 4400x, under different scales: 20, 10 and 5 µm.

II.3.2. HDPE and PB-1 microcomposites characterization

II.3.2.1. Dynamic rheological analysis (DRA)

An internal mixer type (BRABENDER PLASTICORDER, Germany) was used to evaluate the crosslinking reaction, compounding, and mixing procedure. The evolution curves of torque over time were observed and documented during the entirety of the mixing procedure, which was set at a duration of 10 min.

II.3.2.2. Mechanical properties

The tensile test was conducted to determine the mechanical strength, stiffness (Young's modulus), tensile and elongation at break parameters of both the neat resins, Diatomaceous earth-filled and RXR modified micro-composites. Specimens with a dumbbell shape were subjected to testing using a JJ-TEST universal tensile testing machine at a strain rate of 25 mm/min under atmospheric conditions, following the guidelines of ASTM D638. The resilience of V-notched rectangular-shaped specimens was examined using a 5 Joules hammer and an instrumented impact testing machine from INSTRON, according to ASTM E2248 (Charpy).

II.3.2.3. Differential scanning calorimetry (DSC)

The DSC was used to assess the crystallinity, melting, and crystallization characteristics. The NETZSCH DSC 200 F3 differential scanning calorimetry instrument was used to analyze samples weighing 15 ± 2 mg. The scanning cycle began by erasing the thermal history through a first heating cycle from 30 to 180 °C. The samples were held at this temperature for 2 min before being cooled to room temperature at a rate of 10 °C/min. Following a time of stabilization lasting 2 min, a subsequent heating cycle was initiated, reaching a temperature of 190 °C at a heating rate of 10 °C /min.

II.3.2.4. Thermogravimetric analysis (TGA)

The thermal endurance and weight loss rate were assessed by thermogravimetric analysis (TGA). The TA UNIVERSAL ANALYSIS 2000 thermogravimetric analysis device was used to evaluate samples weighing 15 ± 2 mg. The temperature was increased from 20 to 600 °C at a heating speed of 50 °C/min in an inert environment (N_2).

III.3.2.5. Fourier transform infrared (FTIR)

The crystal structure modifications of the neat resins, Diatomaceous earth-filled and RXR modified micro-composites, as well as the various functional groups that may be formed during the reactive extrusion process were assessed using FTIR test. The Shimadzu LabSolutions IR spectroscopy device was used to evaluate compression-molded thin films within the wavenumber range of 4000 to 450 cm^{-1}.

II.3.2.6. Wide angle X-Ray scattering (WAXS)

The WAXS test was used to examine the morphology and the crystal structure modifications of the neat resins, Diatomaceous earth-filled micro-composites, both in the absence and the presence of the RXR agent. BRUKER X-ray diffraction pattern instrument was used to test thin film samples. The apparatus operated at a current of 35 mA and a voltage of 40 kV, emitting CuK± radiation with a wavelength of 0.1541874 nm. The scanning angle ranged from 6 to 60 °, with a step size of 2θ = 0.037 °.

II.3.2.7. Scanning electronic microscopy (SEM)

SEM analysis was used to examine the morphology and dispersion of Diatomaceous earth into the matrix, as well as the topography of both the neat resins, Diatomaceous earth-filled and RXR modified micro-composites. Neoscope JCM-5000 scanning electron microscope was used to scan the gold coated samples at a magnification of 4400x, under two scales of 5, 20 and 50 µm.

CHAPTER III. ENHANCING HIGH DENSITY POLYETHYLENE (HDPE) PERFORMANCE WITH DIATOMACEOUS EARTH FILLER AND A NOVEL REVERSIBLE CROSSLINKING REACTION AGENT (RXR)

Chapter III. Optimizing High-Density Polyethylene (HDPE) performance: Utilizing Diatomaceous earth filler and an innovative Reversible Crosslinking Reaction agent (RXR)

III.1. Results and discussion

III.1.1. Diatomaceous earth characterization

III.1.1.1. Particle size distribution

Characterized by an average water absorption behavior and a porosity of 7% [1], along with a micron to submicron size. The particle size and particle size distribution have a great impact on the mechanical properties of polymeric composites and since the smaller the size the better the interactions are and the higher the reinforcement effect on the composite is [2]. the particle size and their distribution within the matrix is a key factor in determining the composite final properties. **Fig III.1** represent the particle size distribution as was measured by the laser scattering particle size distribution analyzer after the careful milling and sieving of the pristine Diatomaceous earth. The mean particles diameter (d_{50}) was measured to be 16 µm.

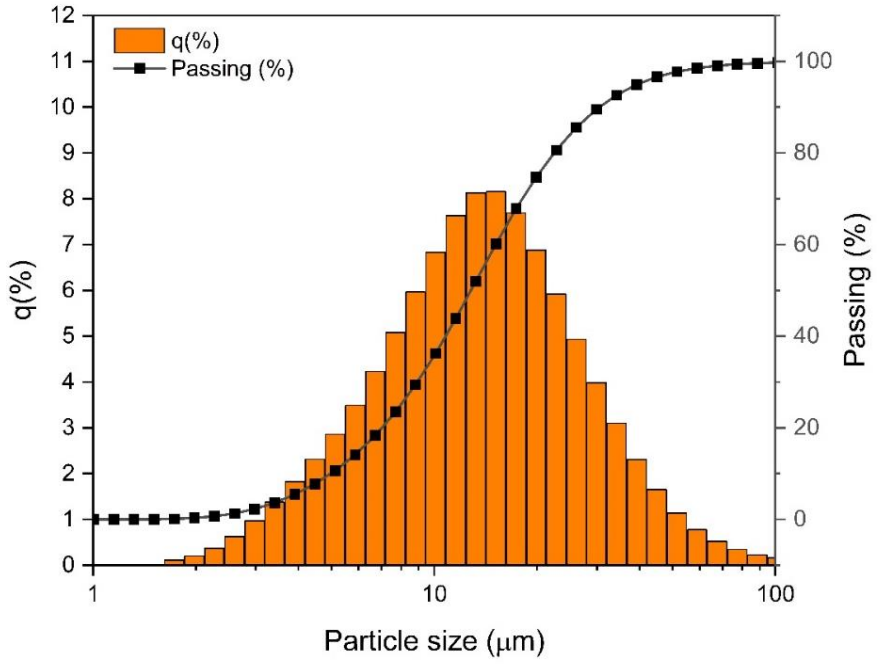

Fig III.1. Diatomaceous earth particle size distribution.

III.1.1.2. Fourier Transform Infrared (FTIR)

The powdered pristine Diatomaceous earth was analyzed by FTIR as illustrated in **Fig III.2**, where the characteristic peaks were clearly seen at 3620, 1437, 997, 797 and 460 cm^{-1}. The vibrational band at 1437 cm^{-1} represents the vibrational motion of carbonate, while the bands at 997 and 460 cm^{-1} are characteristic bands of Si-O-Si bond stretching and bending, respectively. The band at 3620 cm^{-1} is due to the stretching vibration of the hydroxyl groups in physically adsorbed water molecules on the surface of the Diatomaceous earth particles (silanol group Si-OH). The stretching motion of Si-O-Al is related to the band at 797 cm^{-1} [3].

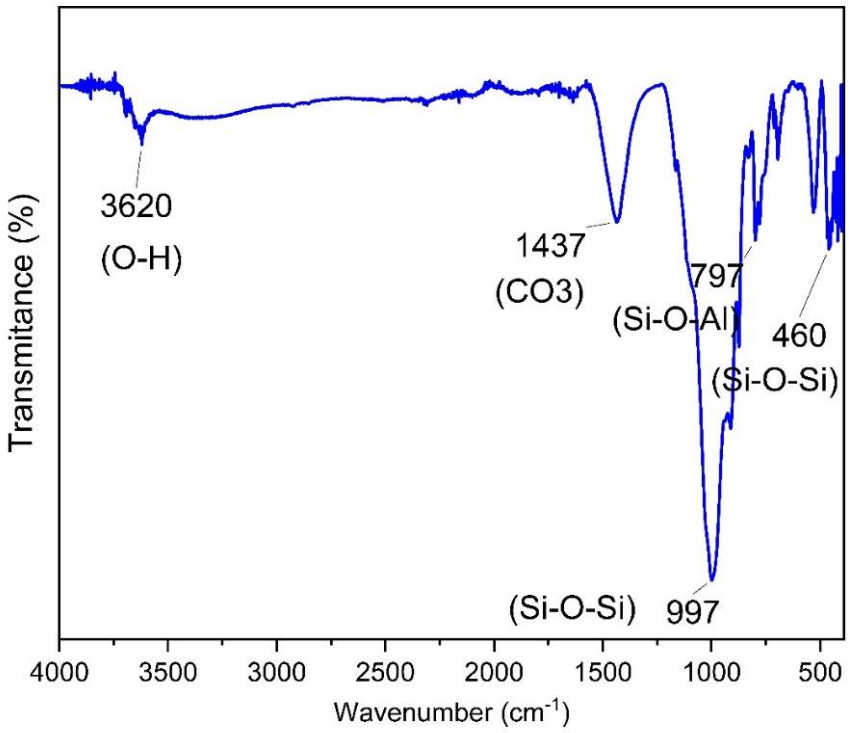

Fig III.2 FTIR spectrum of pristine Diatomaceous earth.

III.1.1.3. Scanning Electron Microscopy (SEM)

An insight was provided about the morphology and microstructure of the obtained Diatomaceous earth samples by means of SEM characterization. The microscopic pictures revealed the existence of intact Diatomaceous earth skeletons whose framework structure is composed of Diatomaceous earth shells represented by various diatom morphological types as can be seen from **Fig III.3**. The SEM observation clearly confirmed the presence of a well-defined and mostly preserved porous structure, which is an important parameter and key medium for any adsorption process, the porous shells consisting mainly of SiO_2 groups. It can be also inferred that the Diatomaceous earth samples are rich

in two classes of diatoms: centric and pennate, and large void volumes. Each frustule of diatom contains areolae due to its high porosity, and the size and disposition of these areolae vary with the species nature [3].

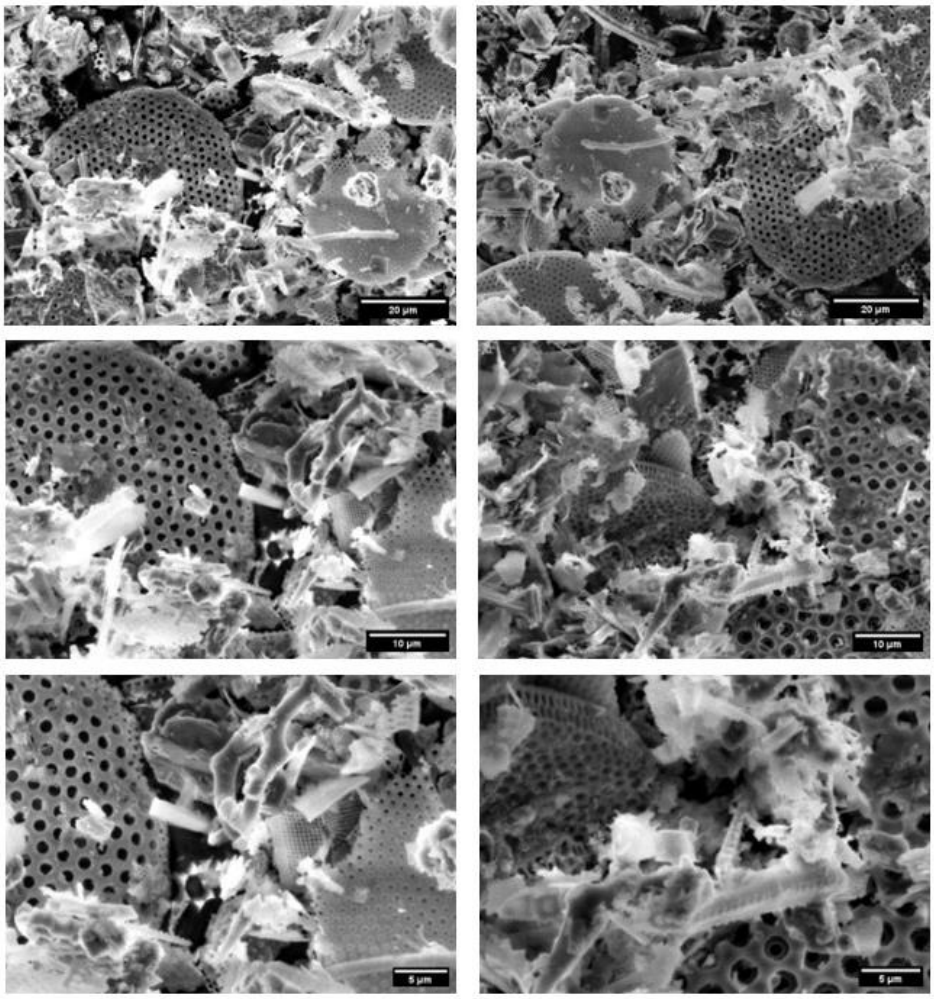

Fig III.3. SEM micrographs of pristine Diatomaceous earth.

III.1.2. HDPE/Diatomaceous earth microcomposites characterization

III.1.2.1. Dynamic rheological analysis (DRA)

The figure clearly illustrates that the addition of both the Diatomaceous earth filler and RXR agent to the HDPE resin results in distinct behavior in terms of torque measurement and, therefore, the viscosity of the resin. During the initial phase of the mixing operation, the torque of the pure HDPE material initially increased until it reached a peak **(D)**, after which it decreased and eventually stabilized at a constant level **(C)**, as depicted in **Fig III.4**. The initial rise is associated with the amalgamation of the solid plastic pellets prior to reaching the point of total liquefaction, as indicated by the plateau [4]. The systems comprising Diatomaceous earth and the RXR agent exhibit distinct

behavior compared to the pure HDPE. Both systems exhibit torque fluctuations during the initial 1-2 minutes, followed by an increase to a maximum point **(D)**. Subsequently, the torque decreases to a point **(A)** before rising again to another maximum torque point **(B)** in the case of the RXR agent-modified samples. Finally, the torque stabilizes on a plateau **(C).** The initial rise **(D)** represents the combined effects of feeding, friction, and surface melting of the solid plastic pellets, while point **(A)** corresponds to the full melting of the microcomposites [5]. The maximum torque attained at point **(B)** serves as a definitive validation of the crosslinking process, indicating the highest degree of crosslinking. Moreover, the decrease in torque after reaching the maximum degree of crosslinking at point **(B)** is attributed to the partial breakdown of the formed network, as previously shown in other studies [4, 6–8]. A state of balance is achieved, shown by a flat and stable region **(C),** which corresponds to the ultimate viscosity of the neat HDPE resin and its microcomposites.

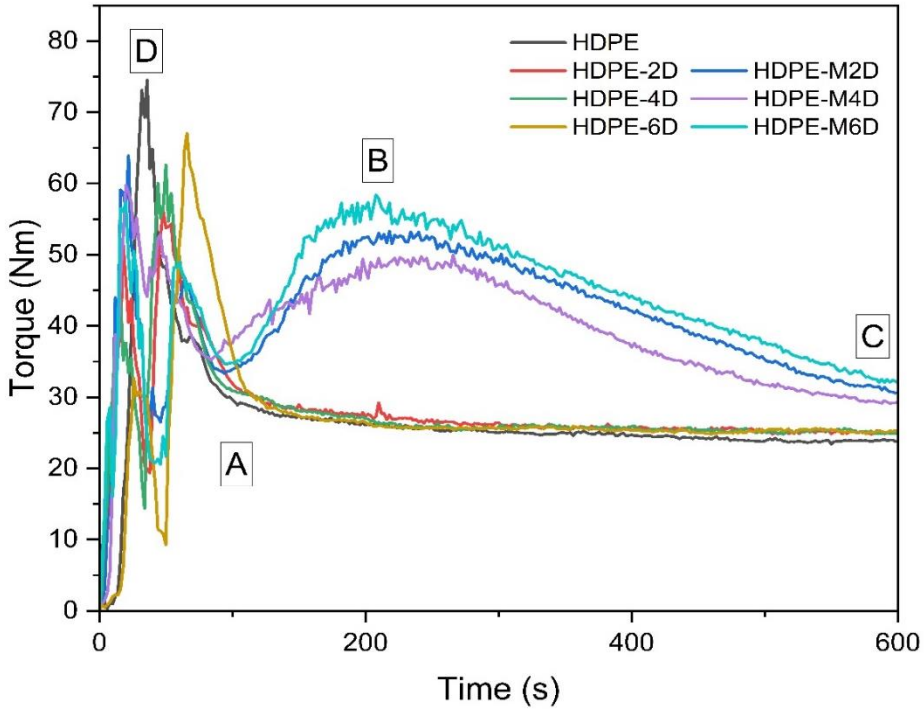

Fig III.4. Torque variation with time of neat and RXR agent modified HDPE/Diatomaceous earth micro-composites.

III.1.2.2. Mechanical properties

III.1.2.2.1. Tensile properties

The use of fillers in a polymeric material has the potential to significantly modify the mechanical characteristics of the final product. Due to the disparity in surface energy between the two materials, the filler particles do not naturally stick to the polymer surface. Instead, they have a tendency to clump

together if not treated. Consequently, this might lead to a decrease in mechanical strength [9]. The composites examined in this study were subjected to a typical tensile test at a rate of 25 mm/min in order to evaluate their attributes, including tensile strength, stress and strain at failure and the stiffness. The results are presented in **Table III.1**, whereas **Fig III.5 (a)** illustrates the stress-strain curves of plain HDPE, as well as RXR-modified and unmodified HDPE with varying Diatomaceous earth weight fractions. **Fig III.5 (b, c** and **d),** represent the variation of the stress and strain of both the unmodified and RXR-modified microcomposites at 2, 4 and 6 wt% of the Diatomaceous earth content, respectively. A noticeable decrease in both the stress and strain at failure is noticed with increase of the Diatomaceous earth content as can be seen from **Fig III.5 (b, c** and **d).** This decrease is a result of the stress concentration around the particles of the filler material, which is known as the "stress concentration phenomenon" [10] yielded from the poor interfacial interactions between the filler and the HDPE/Diatomaceous earth matrix surfaces. The addition of the RXR agent significantly reduced the strain in all the systems under investigation, providing evidence of the crosslinking reaction based on the DRA data. However, the stress at failure was significantly enhanced. In contrast, the stiffness was slightly decreased with the addition of Diatomaceous earth filler, as indicated by the measurements in **Table III.1.** This decrease if probably attributed to the low content of the Diatomaceous earth, its low density and porosity or its pseudo-lubricating effect.

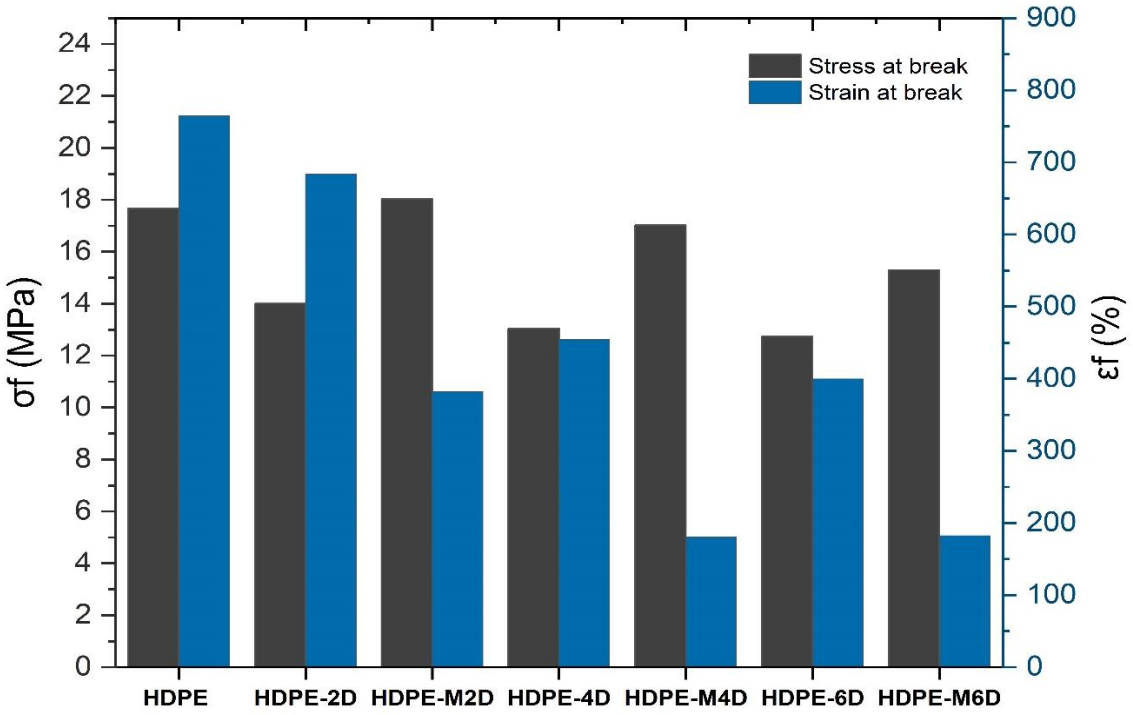

Fig III.5. Tensile stress & strain results of both the unmodified and modified HDPE/Diatomaceous earth microcomposites.

III.1.2.2.2. Impact properties

The changes in impact strength of the neat and the RXR-modified and unmodified HDPE microcomposites with varying Diatomaceous earth fractions, is illustrated in **Fig III.6**. The incorporation of the Diatomaceous earth filler induced a decrease in the impact strength of the HDPE/ Diatomaceous earth microcomposites, as a result of the poor interfacial interactions between the filler and the matrix surfaces, which act as a starting point for the fracture propagation. Nonetheless, the inclusion of the RXR agent in the microcomposites at constant ratios (0.5 wt%), increased the impact strength at lower Diatomaceous earth concentrations, and decreased as the filler content reaches 6 wt%. This increment in the impact strength is attributed to the crosslinking reaction induced by the RXR agent, as was reported in previous studies [11–13] yielding to a more ductile fracture.

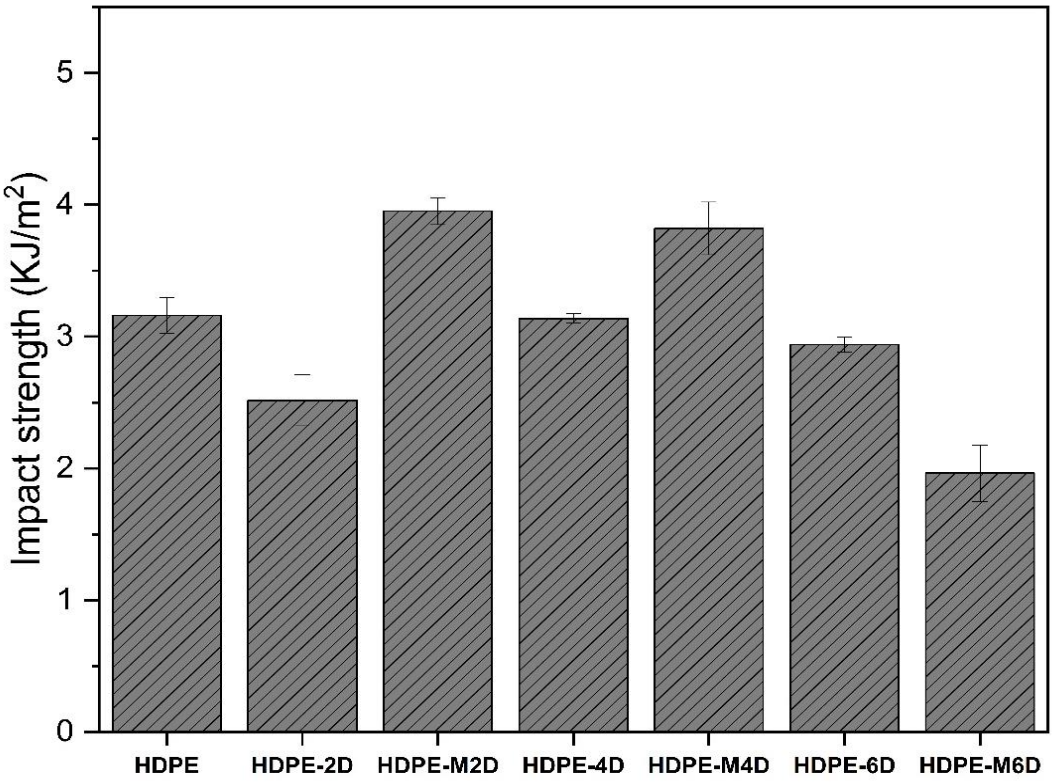

Fig III.6. impact strength of neat HDPE and both the RXR-modified and unmodified HDPE/ Diatomaceous earth microcomposites.

Table III.1. Mechanical properties of neat HDPE and both the RXR-modified and unmodified HDPE/ Diatomaceous earth microcomposites.

	σ_f (MPa)	ε_f (%)	E (MPa)	I (KJ/m^2)
HDPE	17,66	764,71	225,00	3,16
HDPE-2D	14,00	684,00	199,21	2,52
HDPE-M2D	18,03	381,99	171,06	3,95
HDPE-4D	13,05	454,15	181,77	3,14
HDPE-M4D	17,03	180,22	180,98	3,82
HDPE-6D	12,74	399,48	187,71	2,94
HDPE-M6D	15,30	182,26	184,18	2,17

σ_f: Stress at failure; ε_f: strain at failure; **E**: Young's modulus (Stiffness); **I**: impact strength.

III.1.2.3. Thermal characteristics

III.1.2.3.1. Differential scanning calorimetry (DSC)

Thermal characteristics such as melting and crystallization temperatures, heat of fusion and crystallization, and degree of crystallinity were investigated by DSC analysis. The addition of fillers into polymeric materials or their chemical modifications by crosslinking is known to alter their thermal properties. Therefore, DSC was employed to analyze the samples under investigation. **Fig III.7** displays the DSC thermograms for the second heating and cooling cycles of the neat HDPE, as well as the RXR agent-modified and unmodified HDPE/Diatomaceous earth microcomposites. The associated properties of these thermograms are summarized in **Table III.2**. The heating endothermic and cooling exothermic curves exhibit a single prominent peak, as depicted in **Fig III.7 (a)** and **(b)** correspondingly. T_m and T_c represent the temperatures at which melting and crystallization occur at the highest point of their respective peaks. The melting and crystallization enthalpy energies are determined by the area under the curves. As shown in **Table III.2**, the melting and crystallization temperatures remained constant at approximately 139 °C and 108 °C, respectively, regardless of the inclusion of Diatomaceous earth or the presence of the RXR agent. Nevertheless, the heat of fusion slightly increases as the amount of Diatomaceous earth in the mixture rose, particularly at a concentration of 4 wt%. However, in the case of the RXR-modified samples, the fusion energy is noticed to slightly decrease, more particularly at a concentration of 6 wt% of Diatomaceous earth. The crystallization enthalpy exhibits a positive correlation with the Diatomaceous earth content, with a particularly pronounced effect observed at lower concentrations (2 wt%). This suggests an enhancement in the crystal structure and an expansion of the crystal area [14].

The degree of crystallinity is of great importance in semi-crystalline polymers since it is directly related to their mechanical properties [15]. For this reason, crystallinity of the samples was measured by the ratio of the melting enthalpy over the enthalpy energy of 100 % crystalline HDPE which is estimated to be 293 $J.g^{-1}$ [16] using Eq. (1) [15] and the resulted values are listed in **Table III.2**. An increase in the amount of Diatomaceous earth led to a higher degree of crystallinity. This suggests that the Diatomaceous earth particles serve as sites for crystal growth, as observed in a previous study [12]. On the other hand, the presence of the RXR agent appeared to impede crystallization, possibly due to limited chain mobility caused by the three-dimensional network formed by the crosslinking reaction**.** The lamellar thickness was calculated via Eq. (2) [4, 17] and its variation along with the crystallinity is shown in **Fig III.8.** Based on the calculation findings, it was observed that the addition of Diatomaceous earth significantly improved the lamellar thickness, particularly at 2 and 4 wt% Diatomaceous earth content. In these cases, the lamellar thickness doubled compared to the pure HDPE. Nevertheless, the RXR agent decreased the lamellar thickness from 167 to 103 nm. The augmentation of both the degree of crystallinity and the thickness of the lamellae provides evidence of the enhancement in the arrangement of the crystal structure [17]. The degree of crystallinity and lamellar thickness were calculated by **Eq. (1)** and **(2)** respectively.

$$\mathbf{X_c} = \frac{\Delta \boldsymbol{Hm}}{(\mathbf{1}-\boldsymbol{w}) \times \Delta \boldsymbol{H°m}} \quad \ldots\ldots\ldots\ldots \mathbf{(1)}$$

$\mathbf{X_c}$: Degree of crystallinity

w: Weight fraction of Diatomaceous earth

$\mathbf{\Delta H°_m}$: Heat of fusion of 100% crystalline HDPE ($\mathbf{293\ J.g^{-1}}$)

$\mathbf{\Delta H_m}$: Measured heat of fusion

$$\mathbf{L_c} = \frac{\mathbf{2}\boldsymbol{\sigma e} \times \boldsymbol{Tm0}}{\Delta \boldsymbol{Hm0} \times (\boldsymbol{Tm0}-\boldsymbol{Tm})} \quad \ldots\ldots\ldots\ldots \mathbf{(2)}$$

$\mathbf{\sigma_e}$: The surface energy per unit area of the base plane ($\mathbf{9.3 \times 10^{-2}\ J.m^{-2}}$)

$\mathbf{T_m}$: The melting peak from DSC spectrum (**K**)

$\mathbf{T_{m0}}$: The equilibrium melting of infinite thick crystal (**414.6 K**)

$\mathbf{\Delta H_{m0}}$: The melting enthalpy per unit volume crystal ($\mathbf{2.88 \times 10^{8}\ J.m^{-3}}$)

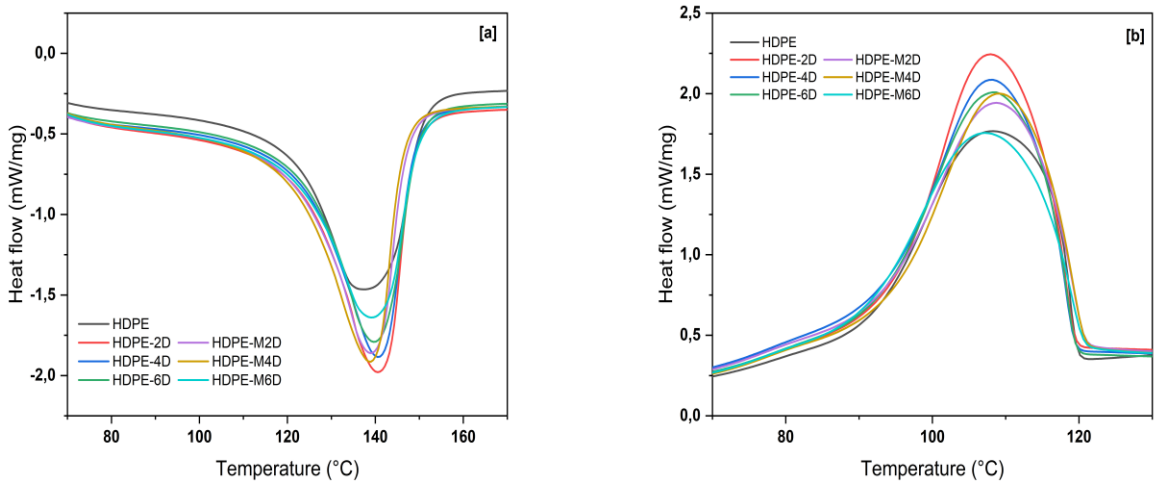

Fig III.7. DSC curves of neat HDPE and both the RXR-modified and unmodified HDPE/Diatomaceous earth microcomposites for melting **(a)** and crystallization measurement **(b)**.

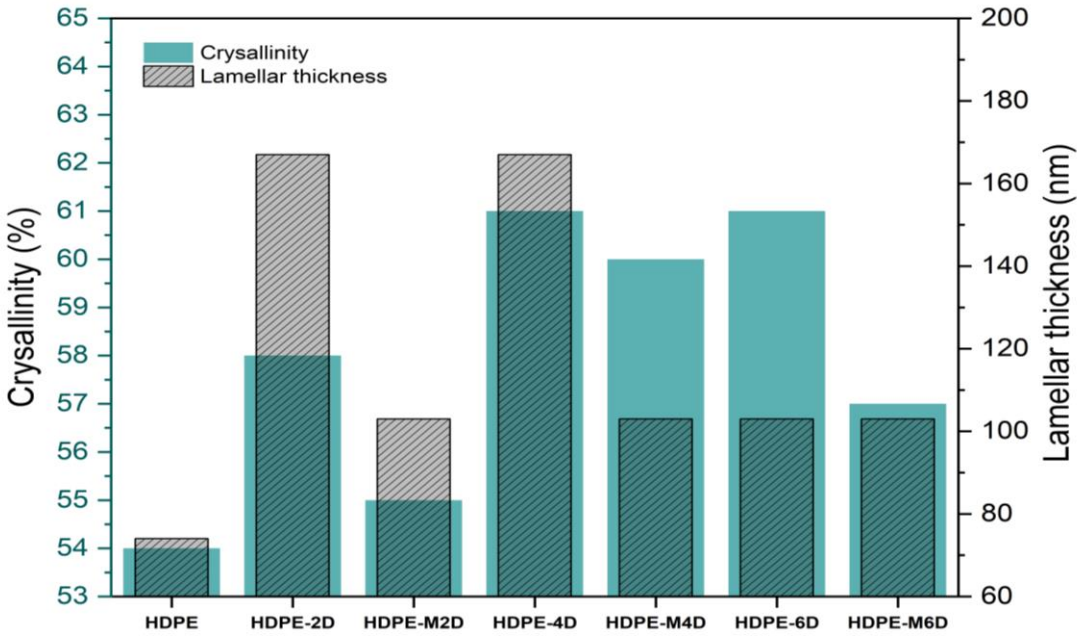

Fig III.8. Crystallinity and lamellar thickness of neat HDPE and both the RXR-modified and unmodified HDPE/Diatomaceous earth microcomposites.

Table III.2. Melting and crystallization characteristics of neat HDPE and both the RXR-modified and unmodified HDPE/Diatomaceous earth microcomposites.

	T_{m0} (°C)	T_m (°C)	ΔH_m ($J.g^{-1}$)	T_{c0} (°C)	T_c (°C)	ΔH_c ($J.g^{-1}$)	X_c (%)	L_c (nm)
HDPE	117	138	159	121	108	170	54	74
HDPE-2D	120	140	167	120	107	181	58	167
HDPE-M2D	118	139	159	121	108	161	55	103
HDPE-4D	120	140	171	120	108	173	61	167
HDPE-M4D	116	139	169	122	109	167	60	103
HDPE-6D	120	139	167	122	108	173	61	103
HDPE-M6D	117	139	157	122	107	150	57	103

III.1.2.3.2. Thermogravimetric analysis (TGA)

The TGA and DTG thermograms of the neat HDPE, as well as the modified and unmodified HDPE/ Diatomaceous earth microcomposites are displayed in **Fig III.9**, and the relevant thermal properties are summarized in **Table III.3**. The examined systems undergo a one-step decomposition process, which is characterized by a single slope curve. The composites have excellent thermal stability, as seen by a plateau in the temperature range from room temperature to 470 °C. Beyond this point, the curve sharply declines, leading to the full disintegration of the polymeric matrix at 502 °C. According to results from **Table III.3**, the addition of Diatomaceous earth or the presence of the RXR agent did not affect the initial (T_0) and final (T_f) decomposition temperatures. This suggests that the thermal stability of the systems did not change, which goes against the results of K. Sever's study [18], at which it was discovered that the inclusion of Diatomaceous earth caused a loss in thermal stability of nearly 7 %. The temperature at the maximum decomposition rate (T_{DTG}) remained consistent at approximately 488 °C, whereas the decomposition rate dropped in all instances.

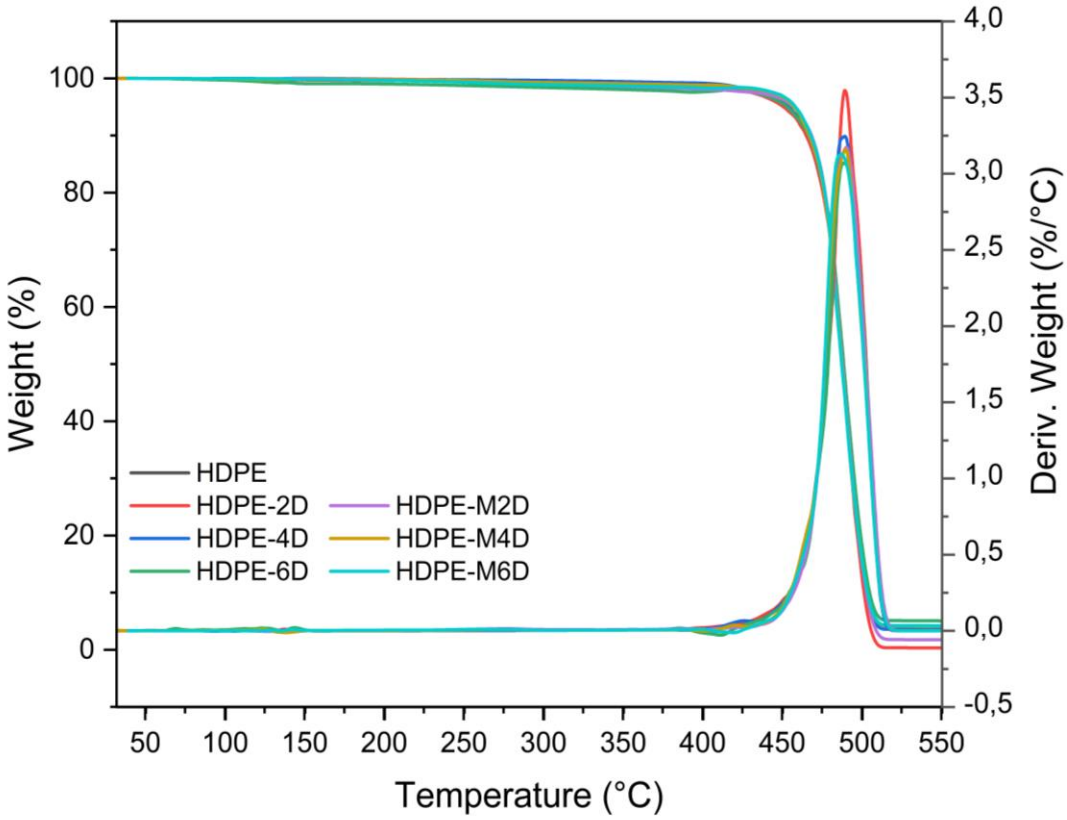

Fig III.9. TGA and DTG thermograms of neat HDPE and both the RXR-modified and unmodified HDPE/ Diatomaceous earth microcomposites.

Table III.3 TGA and DTG characteristics of neat HDPE and both the RXR-modified and unmodified HDPE/ Diatomaceous earth microcomposites.

	TGA				**DTG**	
	T_0 (°C)	T_f (°C)	T_{50} (°C)	t (min)	T_{DTG} (°C)	dwt [%/min]
HDPE	471	501	488	23.40	488	78.50
HDPE-2D	465	499	488	23.94	490	64.59
HDPE-M2D	472	503	488	23.31	490	67.02
HDPE-4D	473	502	488	23.61	490	66.93
HDPE-M4D	471	502	487	23.43	490	64.91
HDPE-6D	473	504	488	23.07	490	63.29
HDPE-M6D	473	502	487	23.05	489	64.81

III.1.2.4. Structural and morphological properties

III.1.2.4.1. Fourier transform infrared (FTIR)

The FTIR spectra of the pure HDPE microcomposites and the HDPE microcomposites treated with the RXR agent, with different weight percentages of Diatomaceous earth, are shown in **Fig III.10.** The bands observed at 720, 1472, and 2900 cm^{-1} are distinctive features of the HDPE resin. The presence of a peak at 720 cm^{-1} corresponds to the rocking vibrations of the CH_2 group and indicates the crystalline nature of the HDPE. Furthermore, the bands observed at 1470 and 2900 cm^{-1} are associated with the deformation vibration of the CH_2 group and the stretching movement of the CH group, respectively [19]. The introduction of Diatomaceous earth filler to the HDPE resin resulted in the emergence of distinct bands at wavenumbers 470, 517, 876, and 1088 cm^{-1}. The bands at 470 and 517 cm^{-1} represent the bending and stretching of (Si–O) bonds, respectively. The band at 876 cm^{-1} corresponds to the vibration movement of (S-OR). The broad band at 1088 cm^{-1} corresponds to the siloxane structure (Si–O–Si). The intensity of these bands increases as the Diatomaceous earth content increases. The vibrational bands at 909 and 990 cm^{-1}, which are associated with the bending motion of a terminal vinyl group (–CH=CH_2) [20, 21] appeared to significantly diminish in the samples treated with the RXR agent. Conversely, new bands were observed at 960 cm^{-1}, corresponding to the trans-vinylene absorption band (–CH=CH–) [4] as depicted in **Fig III.11.** The absence of the terminal vinyl group and the presence of the A trans-vinylene groups are evidence of the double bond opening and the development of the three-dimensional network, indicating that the crosslinking process has taken place, as confirmed by the DRA results. Typically, when crosslinking cases are treated with DCP, acetophenone, cumyl alcohol, and α-methylstyrene, byproducts are formed during the crosslinking reaction. These byproducts correspond to the following functional groups: styryl, carbonyl (C=O), and hydroxyl (–OH). These functional groups can be identified by the bands at 1600, 1680, and 3371 cm^{-1}, respectively [22]. The intensity of these bands correlates directly with the quantity of byproducts formed during the crosslinking operation, indicating a higher crosslinking density. However, the crosslinking method employed in this study does not solely consume the DCP, but also utilizes an accelerator (TMTD) and sulphur. Consequently, the intensity of the three bands at 1600, 1680, and 3371 cm^{-1} remained unchanged in all samples, including those containing the RXR. The crosslinking reaction results in the formation of bands at specific wavelengths, namely 475, 500, 875, 965, 1110, and 1150 cm^{-1}. These bands correspond to the vibration of aryl-S-S-aryl, the bonding of disulfide, and the swinging of N-H. They are observed in a similar study and are caused by the reaction with the accelerator. Additionally, the Diatomaceous earth vibration movements overlap with the trans-vinylene absorption band, C = S stretching band, and C-S band.

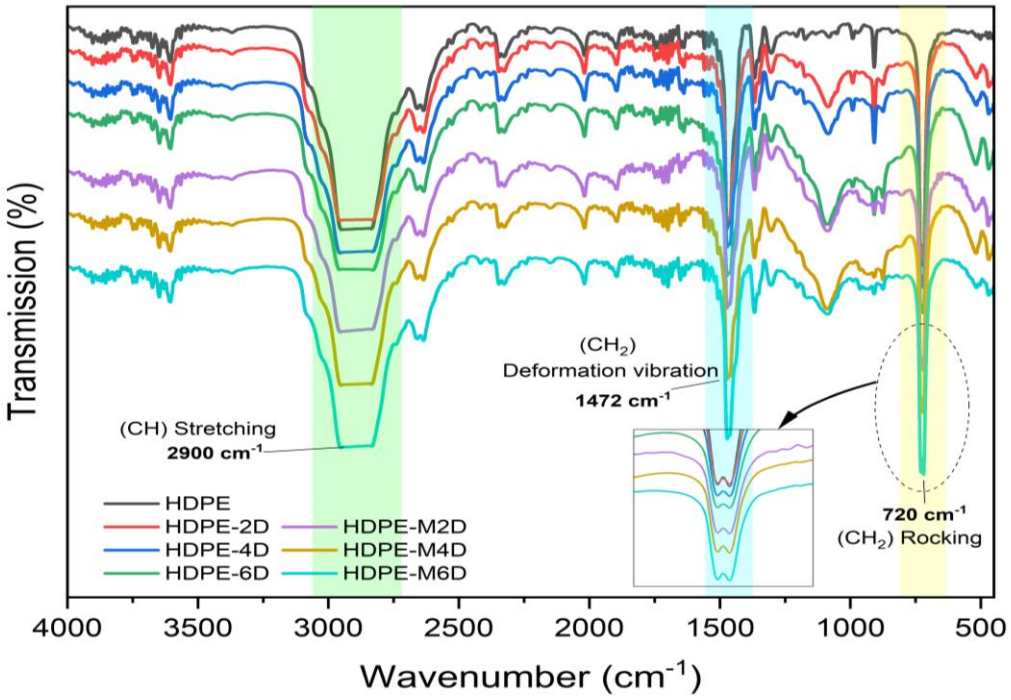

Fig III.10 FTIR spectrums of neat HDPE and both the RXR-modified and unmodified HDPE/ Diatomaceous earth microcomposites

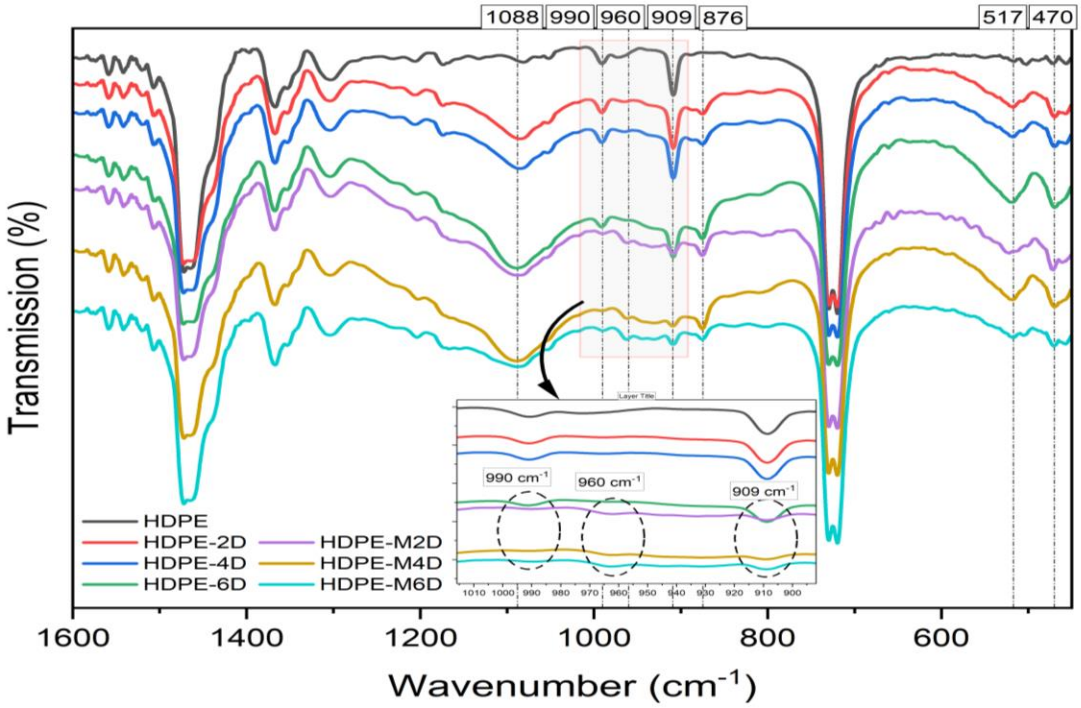

Fig III.11. FTIR spectrums in the range 450 to 1600 cm^{-1} of neat HDPE and both the RXR-modified and unmodified HDPE/ Diatomaceous earth microcomposites

III.1.2.4.2. Wide angle X-Ray scattering (WAXS)

The structure, crystallite size, and crystallinity of the microcomposites were examined using a wide-angle X-ray spectrum (WAXS). **Fig III.12,** depicts the WAXS spectra of the pure and RXR agent-modified high-density polyethylene (HDPE) at different weight fractions of Diatomaceous earth. The spectrum has two highly defined sharp peaks at 2θ = 21° and 2θ = 23°, which correspond to the (110) and (200) crystallographic planes, respectively. Incorporating Diatomaceous earth results in the emergence of a wide halo peak at approximately 2θ = 12.5°, which is associated with the amorphous silica present in the distinctive structure of Diatomaceous earth. The intensity of this peak increases as the amount of Diatomaceous earth used is increased. The addition of both Diatomaceous earth and the RXR agent did not appear to modify the composition of the HDPE and the various microcomposites. Nevertheless, the strength of their intensity is evidently influenced, indicating a modification in the crystallinity. The degree of crystallinity, interplanar spacing, and crystallite size were determined and the findings are presented in **Table III.4**. The degree of crystallinity is quantified as the proportion of the crystalline region to the combined area of both the crystalline and amorphous regions, as indicated by **Eq. (3)** [15]. The peaks were fitted using the Gaussian-Lorentz equation and the deconvolution method, as shown in **Fig III.13**. Similarly, in line with the DSC findings, the presence of Diatomaceous earth leads to an increase in crystallinity. However, the RXR agent appears to impede the crystallization process, as evidenced by the data presented in **Table III.4**. The inclusion of both Diatomaceous earth and the RXR agent did not alter the interplanar spacing (d), which was determined using Bragg's equation **Eq. (4)** [4, 15]. On the other hand, the size of the crystallites was determined using the Scherrer formula **Eq. (5)** [4, 15]. It was seen that the integration of Diatomaceous earth resulted in a very minor drop in crystallite size, which was further reduced in the presence of the RXR agent. Previous study [12] yielded comparable findings, noting that the Diatomaceous earth had the effect of reducing the size of crystallites.

The crystallinity degree, interplanar spacing (d) and the size of the crystallites were calculated using **Eq. (3), (4)** and **(5)** respectively.

$$X_c^{WAXS} = A_{cr} / (A_{cr} + A_{am}) \quad \text{..... (3)}$$

X_c: degree of crystallinity

A_{cr}: Crystalline area

A_{am}: Amorphous area

$$n \times \lambda = 2d \times \sin\theta \quad \text{..... (4)}$$

ʎ: W-ray wavelength (1,5406 Å)

d: inter planar spacing

θ: Bragg's angle in degree

$$\mathbf{L_c} = \frac{K\lambda}{\beta \times cos\theta} \quad \text{..... (5)}$$

$\mathbf{L_c}$ = Crystal size (nm)

β = Full width at half maxima in radian

θ = Bragg's angle in radian

K: Scherrer constant (0,94)

ʎ: W-ray wavelength (1,5406 Å)

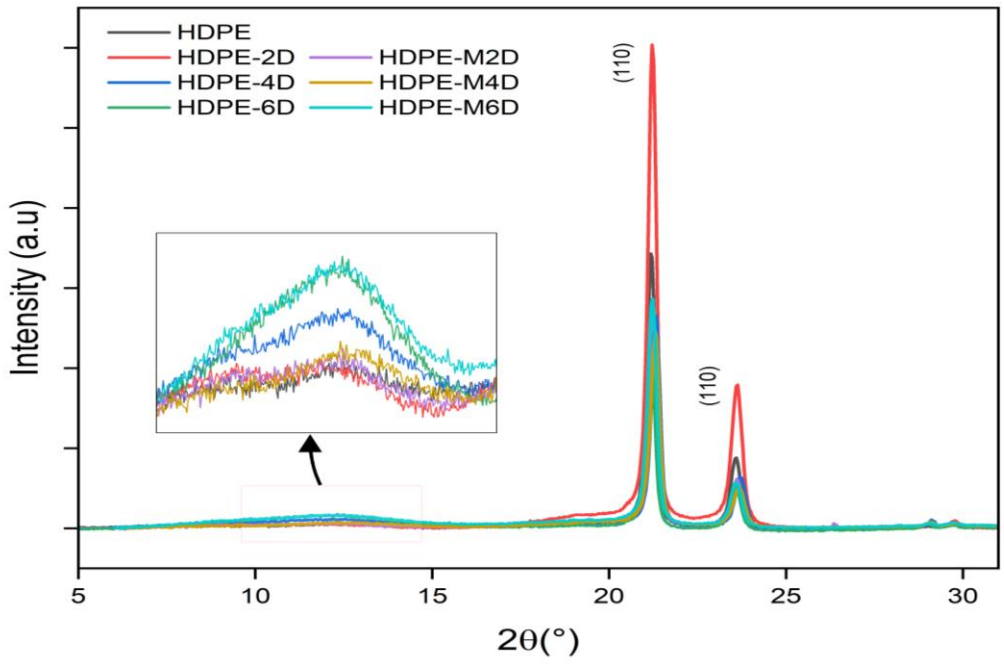

Fig III.12 WAXS spectrums of neat HDPE and both the RXR-modified and unmodified HDPE/ Diatomaceous earth microcomposites

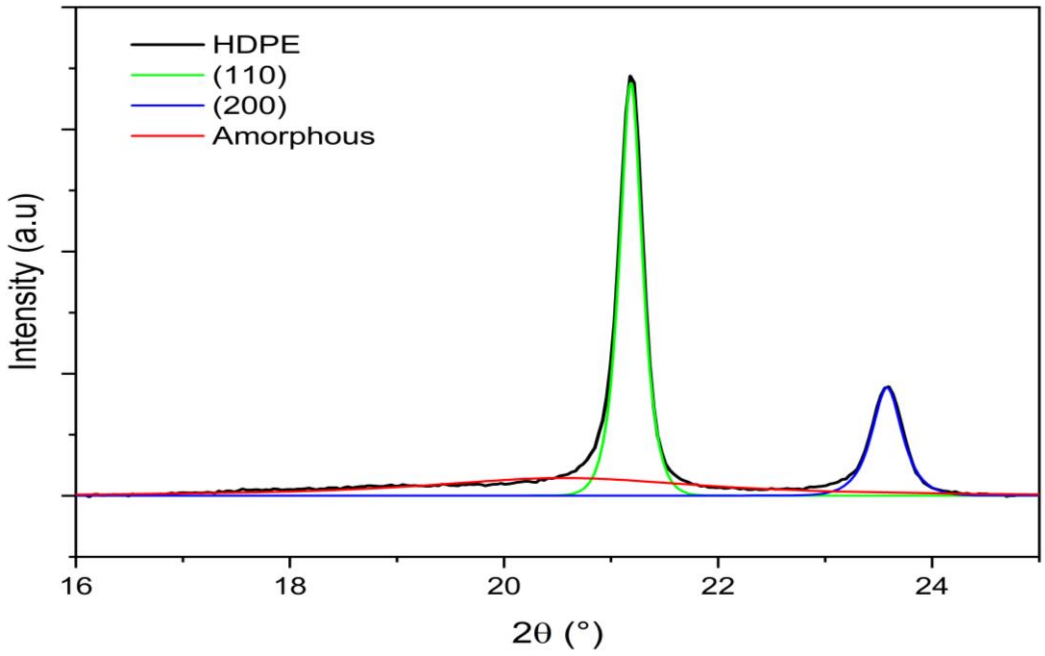

Fig III.13 XRD peak deconvolution of neat HDPE.

Table III.4 WAXS characteristics of neat HDPE and both the RXR-modified and unmodified HDPE/ Diatomaceous earth microcomposites

	$2\theta_{(110)}$	d_{110} (nm)	β_{110}	L_{110} (nm)	$2\theta_{(200)}$	d_{200} (nm)	β_{200}	L_{200} (nm)	L_{avrg} (nm)	X_c^{WAXS} (%)
HDPE	21,18	24,02	0,30	28	23,58	21,60	0,38	22	25	68
HDPE-2D	21,22	23,97	0,32	27	23,60	21,58	0,42	20	23	69
HDPE-M2D	21,22	23,97	0,35	24	23,59	21,59	0,44	19	22	71
HDPE-4D	21,31	23,87	0,33	26	23,70	21,49	0,42	20	23	71
HDPE-M4D	21,29	23,89	0,34	25	23,66	21,53	0,44	19	22	59
HDPE-6D	21,18	24,02	0,32	27	23,56	21,62	0,42	20	23	83
HDPE-M6D	21,21	23,98	0,34	25	23,58	21,60	0,44	19	22	66

III.1.2.4.3. Scanning electronic microscopy (SEM)

The morphology of the plain HDPE microcomposites and the HDPE microcomposites treated with the RXR agent, as well as the dispersion of Diatomaceous earth inside the matrix, were examined using scanning electron microscopy (SEM). **Fig III.14 (a** and **b)** display the micrographs of the microcomposites with a Diatomaceous earth content of 2 wt% at a magnification of 50 and 20 µm, respectively. While **Fig III.14 (c** and **d)** exhibit the micrographs of the samples containing the RXR agent with the same Diatomaceous earth content at a magnification of 20 and 5 µm, respectively. Upon

examination of the micrographs, it was observed that the surface characteristics of the matrix became more uneven as the concentration of diatomaceous earth rose. The Diatomaceous earth particles can be observed in **Fig III.14 (a** and **b)** forming clusters with diverse forms and sizes. The average length and surface area of these particles, as determined by *ImageJ* Analysis software, are 17 µm and 5 µm^2, respectively. **Fig III.14 (c** and **d)** reveals a porous structure where Diatomaceous earth particles are present within the pores without any interfacial interactions between the two phases. **Fig III.14 (d)** provides a clear example of a 3 µm Diatomaceous earth particle that is observed to be lying in a hole without any interactions with the surrounding matrix. This observation helps to explain the decrease in mechanical strength caused by the inclusion of Diatomaceous earth into the HDPE resin. The reduction in mechanical strength can be directly linked to the stress concentration around the Diatomaceous earth particles because there are no interfacial contacts to facilitate the transfer of applied stress to the microcomposites [18, 23].

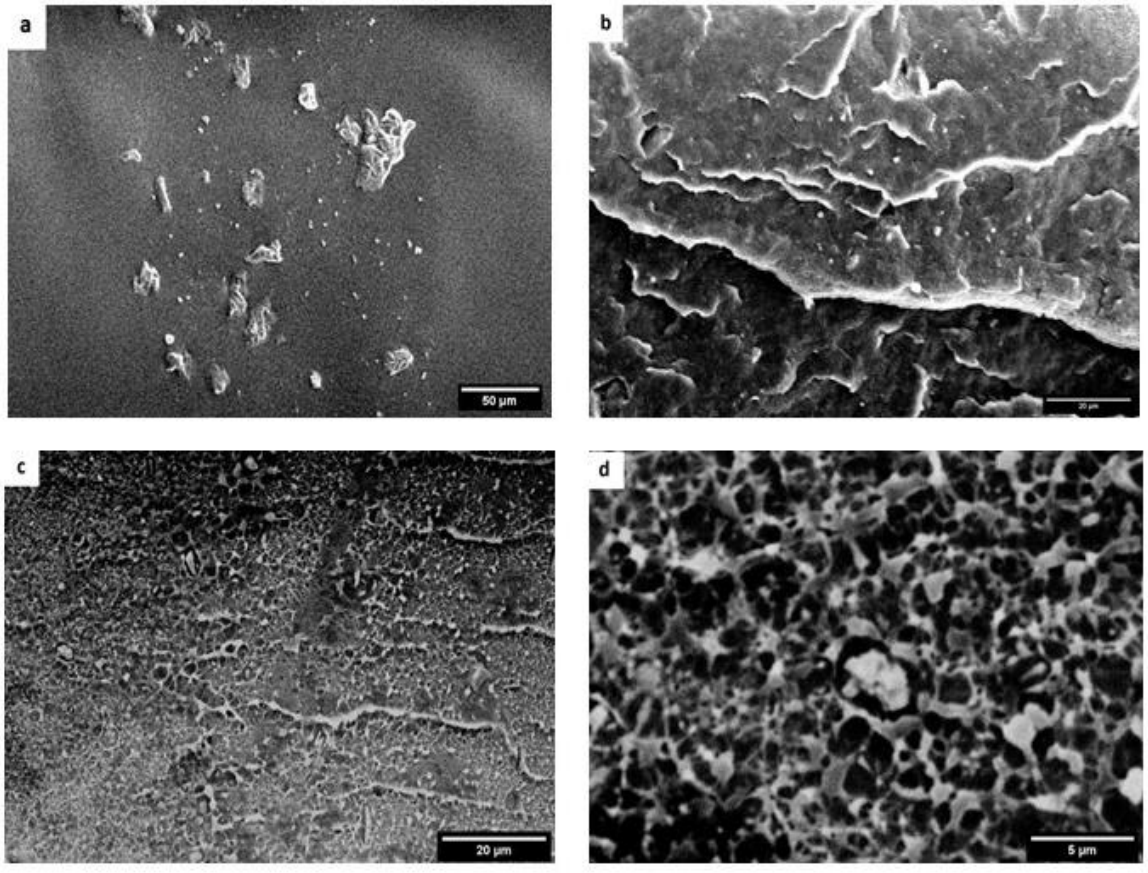

Fig III.14. SEM micrographs of HDPE filled with 2wt% of Diatomaceous earth (**a** and **b**) and RXR-modified samples at 2wt% Diatomaceous earth content (**c** and **d**).

References

[1] Lamamra, A.; Neguritsa, D. L.; Bedr, S.; Reka, A. A. Determination and Quality Classification of Rock Mass of the Diatomite Mine, Algeria. *News Ural State Min. Univ.* 2021, *1* (61), 17–24. https://doi.org/10.21440/2307-2091-2021-1-17-24.

[2] Wu, W. L.; Chen, Z. Modified-Diatomite Reinforced Rubbers. *Mater. Lett.* 2017, *209* (July), 159–162. https://doi.org/10.1016/j.matlet.2017.07.133.

[3] Touina, A.; Chernai, S.; Mansour, B.; Hadjar, H.; Ouakouak, A.; Hamdi, B. Characterization and Efficient Dye Discoloration of Algerian Diatomite from Ouled Djilali-Mostaganem. *SN Appl. Sci.* 2021, *3* (4). https://doi.org/10.1007/s42452-021-04334-9.

[4] Saci, H.; Bouhelal, S.; Bouzarafa, B.; López, D.; Fernández-García, M. Reversible Crosslinked Low Density Polyethylenes: Structure and Thermal Properties. *J. Polym. Res.* 2016, *23* (4), 68. https://doi.org/10.1007/s10965-016-0965-x.

[5] Tariq, A.; Ahmad, N. M.; Abbas, M. A.; Shakir, M. F.; Khaliq, Z.; Rafiq, S.; Ali, Z.; Elaissari, A. Reactive Extrusion of Maleic-Anhydride-Grafted Polypropylene by Torque Rheometer and Its Application as Compatibilizer. *Polymers (Basel)* 2021, *13* (4), 495. https://doi.org/10.3390/polym13040495.

[6] Khellaf, S.; Khoffi, F.; Tabet, H.; Lallam, A.; Bouhelal, S.; Cagiao, M. E.; Benachour, D.; Baltá-Calleja, F. J. Study of IPP Crosslinking by Means of Dynamic and Steady Rheology Measurements. *J. Appl. Polym. Sci.* 2012, *124* (4), 3184–3191. https://doi.org/10.1002/app.34996.

[7] Bouhelal, S.; Cagiao, M. E.; Benachour, D.; Calleja, F. J. B.; Baltá Calleja, F. J.; Calleja, F. J. B. Structure Modification of Isotactic Polypropylene through Chemical Crosslinking: Toughening Mechanism. *J. Appl. Polym. Sci.* 2007, *103* (5), 2968–2976. https://doi.org/10.1002/app.25406.

[8] Bouhelal, S.; Cagiao, M. E.; Di Lorenzo, M. L.; Zouai, F.; Khellaf, S.; Tabet, H.; Benachour, D.; Calleja, F. J. B. Study of Rheological and Mechanical Properties of Ternary Blends of IPP/LDPE/EPDM. *J. Polym. Eng.* 2012, *32* (3). https://doi.org/10.1515/polyeng-2011-0130.

[9] Wang, K. Y.; Sun, Q. J.; Liu, Y.; Lu, J. Thermal Behavior, Mechanical Property and Microstructure of Low-Density Polyethylene Filled by Diatomite. *Appl. Mech. Mater.* 2014, *633–634*, 413–416. https://doi.org/10.4028/www.scientific.net/AMM.633-634.413.

[10] Zhan, F.; Chen, N. C.; Zhang, X. H.; Huang, B.; Wu, Z. N.; Zhu, Q. Abrasion Properties and Thermal Stabilities of Poly(Vinylchloride)/Diatomite Composites. *Adv. Mat. Res.* 2014, *833*, 317–321. https://doi.org/10.4028/www.scientific.net/AMR.833.317.

[11] Bouhelal, S.; Cagiao, M. E.; Khellaf, S.; Benachour, D.; Baltá Calleja, F. J.; Calleja, F. J. B. Structure and Properties of New Reversibly Crosslinked IPP/LDPE Blends. *J. Appl. Polym. Sci.* 2008, *109* (2), 795–804. https://doi.org/10.1002/app.28194.

[12] Hu, S.-F.; Zhu, X.-B.; Hu, W.; Yan, L.; Cai, C. Crystallization Behaviors and Foaming Properties of Diatomite-Filled Polypropylene Composites. *Polym. Bull.* 2013, *70* (2), 517–533. https://doi.org/10.1007/s00289-012-0849-0.

[13] Hichem, R.; Bouhelal, S. Effect of the Chemical Modification of Diatomite/Isotactic Polypropylene Composite on the Rheological, Morphological and Mechanical Properties. *Adv. Mat. Res.* 2023, *1177*, 121–136. https://doi.org/10.4028/p-956acc.

[14] Zhao, Y.; Han, Z.; Xie, Y.; Fan, X.; Nie, Y.; Wang, P.; Liu, G.; Hao, Y.; Huang, J.; Zhu, W. Correlation Between Thermal Parameters and Morphology of Cross-Linked Polyethylene. *IEEE Access* 2020, *8*, 19726–19736. https://doi.org/10.1109/ACCESS.2020.2968109.

[15] Tarani, E.; Arvanitidis, I.; Christofilos, D.; Bikiaris, D. N.; Chrissafis, K.; Vourlias, G. Calculation of the Degree of Crystallinity of HDPE/GNPs Nanocomposites by Using Various Experimental Techniques: A Comparative Study. *J. Mater. Sci.* 2023, *58* (4), 1621–1639. https://doi.org/10.1007/s10853-022-08125-4.

[16] Tarani, E.; Papageorgiou, D. G.; Valles, C.; Wurm, A.; Terzopoulou, Z.; Bikiaris, D. N.; Schick, C.; Chrissafis, K.; Vourlias, G. Insights into Crystallization and Melting of High Density Polyethylene/Graphene Nanocomposites Studied by Fast Scanning Calorimetry. *Polym. Test.* 2018, *67*, 349–358. https://doi.org/10.1016/j.polymertesting.2018.03.029.

[17] Ding, M.; He, W.; Wang, J.; Wang, J. Performance Evaluation of Cross-Linked Polyethylene Insulation of Operating 110 KV Power Cables. *Polymers (Basel)* 2022, *14* (11), 2282. https://doi.org/10.3390/polym14112282.

[18] Sever, K.; Atagur, M.; Altay, L.; Seki, Y.; Uysalman, T.; Sen, I.; Kaya, N.; Guven, A.; Sarikanat, M. Effect of Diatomite Weight Fraction on Morphology, Thermal and Physical Properties of Diatomite Filled High Density Polyethylene Composites. *Acta Phys. Pol. A* 2018, *134* (1), 281–284. https://doi.org/10.12693/APhysPolA.134.281.

[19] Yu, S.; Park, C.; Hong, S. M.; Koo, C. M. Thermal Conduction Behaviors of Chemically Cross-Linked High-Density Polyethylenes. *Thermochim. Acta* 2014, *583*, 67–71. https://doi.org/10.1016/j.tca.2014.03.018.

[20] Pagès, P. Characterization of Polymer Materials Using FT-IR and DSC Techniques. 2005.

[21] Kuptsov, A. H. *Handbook of Fourier Transform Raman and Infrared Spectra of Polymers*; 1998. https://doi.org/https://doi.org/10.1023/A:1008198824934.

[22] Zhao, Y.; Han, Z.; Xie, Y.; Fan, X.; Nie, Y.; Wang, P.; Liu, G.; Hao, Y.; Huang, J.; Zhu, W. Correlation Between Thermal Parameters and Morphology of Cross-Linked Polyethylene. *IEEE Access* 2020, *8*, 19726–19736. https://doi.org/10.1109/ACCESS.2020.2968109.

[23] Gonzalez, L.; Agüero, A.; Quiles-Carrillo, L.; Lascano, D.; Montanes, N. Optimization of the Loading of an Environmentally Friendly Compatibilizer Derived from Linseed Oil in Poly(Lactic Acid)/Diatomaceous Earth Composites. *Materials* 2019, *12* (10), 1–15. https://doi.org/10.3390/ma12101627.

CHAPTER IV. IMPROVING ISOTACTIC POLYBUTENE-1 (PB-1) PERFORMANCE WITH DIATOMACEOUS EARTH FILLER AND A NOVEL REVERSIBLE CROSSLINKING REACTION AGENT (RXR)

CHAPTER IV. IMPROVING ISOTACTIC POLYBUTENE-1 (PB-1) PERFORMANCE WITH DIATOMACEOUS EARTH FILLER AND A NOVEL REVERSIBLE CROSSLINKING REACTION AGENT (RXR)

IV.1. Results and discussion

IV.1.2. PB-1/Diatomaceous earth microcomposites characterization

IV.1.2.1. Dynamic rheological analysis (DRA)

The torque characteristics of PB-1 at different Diatomaceous earth fractions (0.5, 1, 2, and 4 wt%) are depicted in **Fig IV. 1**, taking into account the presence and absence of the RXR agent. The data presented in the figure provides convincing evidence that the incorporation of both the Diatomaceous earth filler and RXR agent into the PB-1 resin yields notable impacts on torque measurement and, consequently, the resin's viscosity. During the first phase of the mixing procedure, the torque of the pure and filled PB-1 exhibited an initial rise until reaching a peak value **(D)**, followed by a subsequent decrease and eventual stabilization at an equilibrium plateau **(C)**, as seen in **Fig IV. 2(a)**. The first rise may be attributed to the amalgamation of the solid plastic pellets prior to the attainment of full melting, as shown by the plateaus [1, 2]. The systems, including the RXR agent, exhibit distinct behavior compared to the pure and filled PB-1, as seen in **Fig IV. 2(b)**. In both systems, it can be noticed that the torque exhibits fluctuations during the first 1-2 minutes, followed by a rise until reaching a maximum point **(D)**. Subsequently, the torque decreases to a point **(A)** before re-elevating to a maximum torque point **(B)**, and finally, it stabilizes at a plateau **(C)**. The initial increment **(D)** is indicative of the processes of feeding, friction, and surface melting of the solid plastic pellets [3], while point **(A)** signifies the full melting of the PB-1 resin. The attainment of the maximum torque at point **(B)** is indicative of the greatest level of crosslinking, providing compelling evidence for the presence of the crosslinking process, as shown in prior studies [1, 4–6]. Furthermore, the observed reduction in torque subsequent to the attainment of maximum crosslinking at point **(B)** might be ascribed to the partial degradation of the established network. The PB-1 resin reaches an equilibrium torque, which is depicted by a plateau **(C)** and indicates the ultimate viscosity.

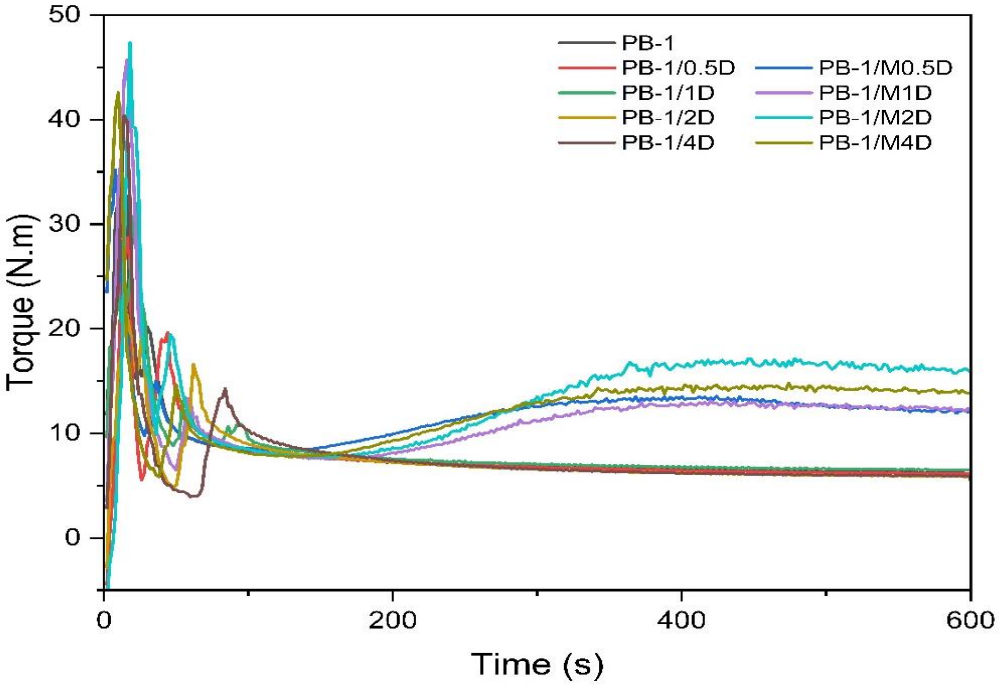

Fig IV. 1. Torque evolution with time of the neat PB-1, PB-1/Diatomaceous earth and RXR modified PB-1/Diatomaceous earth micro composites.

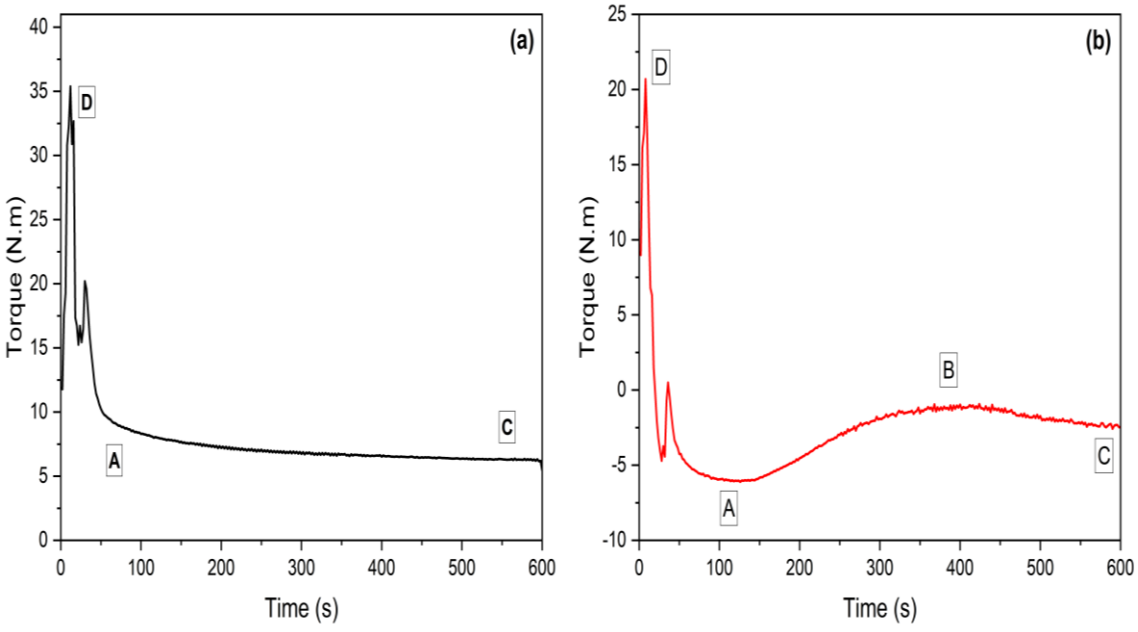

Fig IV. 2. Torque evolution with time of **(a)** Diatomaceous earth filled PB-1, **(b)** RXR modified PB-1/Diatomaceous earth microcomposites.

IV.1.2.2. Mechanical properties

IV.1.2.2.1. Tensile properties

Fig IV.3 depicts the stress and strain curves of the neat PB-1 and PB-1/Diatomaceous earth microcomposites, both in the absence and presence of the RXR agent. From the figure, it is clearly seen that the PB-1 illustrates a rubbery-like deformation, reaching a failure point of up to 1400%. Nonetheless, the addition of both the Diatomaceous earth filler and the RXR agent greatly reduced the stress, and an even more drastic decrease is recorded in the strain at failure, changing the resin's behavior from ductile to brittle. A similar trend was observed when untreated wood powder was added to PB-1 resin [7]. From the measured results summarized in **Table IV.1**, it's clear that the addition of the Diatomaceous earth causes a decrease in both stress and strain due to its incompatibility with PB-1 resin, and even further decreases are noticed by the incorporation of the RXR agent. The decrease in strain at failure in the RXR agent-modified samples is probably due to the crosslinking reaction. The stiffness (Young's modulus), on the other hand, also seems to decrease nearly 50% with both Diatomaceous earth and the RXR agent addition. This scenario may be attributed to the low stiffness of the Diatomaceous earth itself, its porosity, which can act as a stress concentrator [8], its incompatibility with the matrix, or the flexibility of its particles, which is due to the pseudo-lubricating effect generated by the low content of the Diatomaceous earth, resulting in slippage of the methylene chains over one another [9].

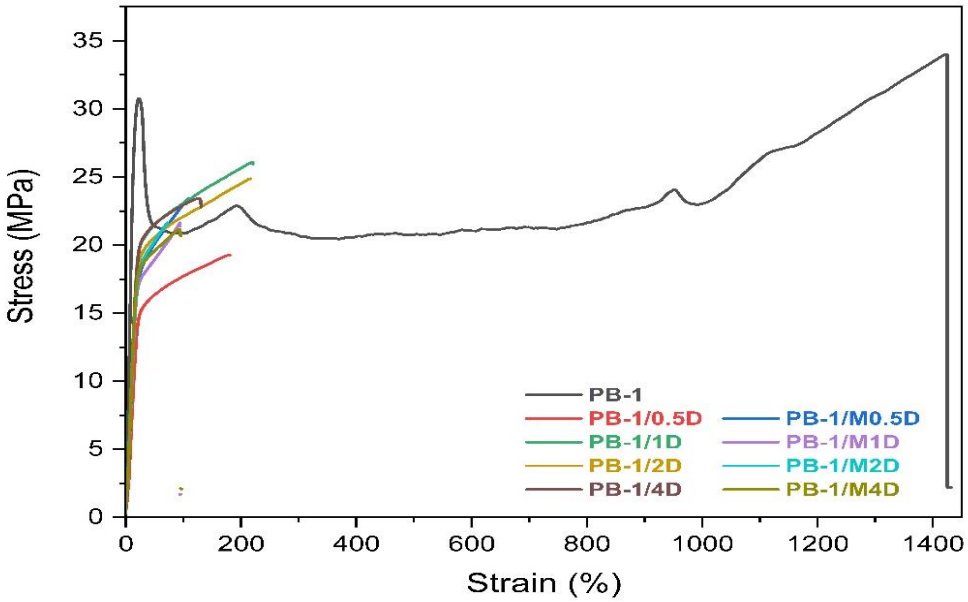

Fig IV. 3. Stress & Strain curve of the neat PB-1, PB-1/Diatomaceous earth and RXR modified PB-1/Diatomaceous earth microcomposites.

IV.1.2.2.1. Impact properties

Neat PB-1 possesses a good resistance to impact due to its softness and elasticity, as can be seen from the measurements in **Fig IV. 4**. When Diatomaceous earth was added to the matrix even in a small ratio of 0.5 wt%, a drastic decrease in resilience of nearly 50% was noticed, and as the Diatomaceous earth content increased, the resilience also slightly increased. The addition of the RXR agent appeared to have no positive effect on resilience, but rather slightly contributed to its reduction. The reduction in impact resistance is probably due to the brittleness behavior of the PB-1 microcomposites, as found from the tensile test, resulting from the filler-matrix poor interfacial interactions, thus leading to stress buildup, which can act as a nucleation site for crack formation [10, 11].

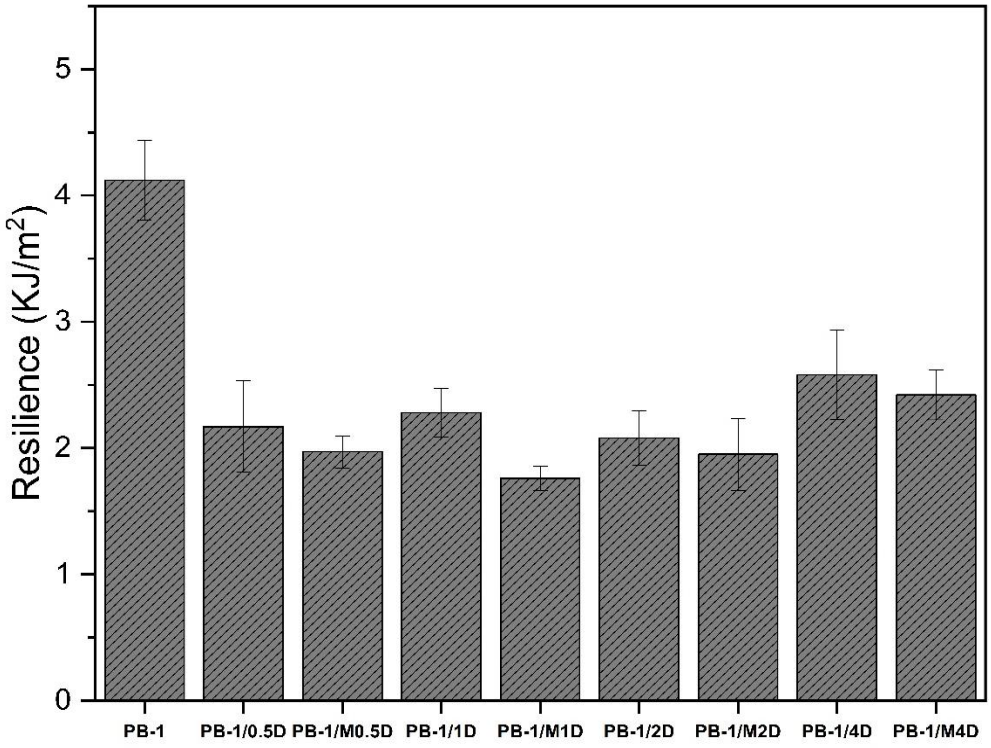

Fig IV. 4. Resilience of neat PB-1 and PB-1/Diatomaceous earth microcomposites both in the absence and the presence the RXR agent.

Table IV.1. Mechanical properties of the neat PB-1 and both the RXR modified and unmodified PB-1/Diatomaceous earth microcomposites.

	σ_f (MPa)	ε_f (%)	$\sigma_{0.2y}$ (MPa)	$\varepsilon_{0.2y}$ (%)	σ_{UTS} (MPa)	ε_{UTS} (%)	E (MPa)	I (KJ/m²)
PB-1	29,790	1319,911	20,750	10,180	30,203	23,451	206.647	4.125
PB-1/0.5D	17,685	166,845	10,124	13,747	17,685	166,845	81.612	2.167
PB-1/M0.5D	20,105	60,332	11,763	12,090	20,356	59,863	104,955	1.968
PB-1/1D	24,378	152,093	13,620	13,478	24,755	149,683	113.084	2.278
PB-1/M1D	19,122	58,601	12,163	12,517	19,597	57,731	106,952	1.765
PB-1/2D	24,143	211,264	11,692	12,471	24,143	211,264	109.185	2.079
PB-1/M2D	20,005	58,638	13,180	14,101	20,332	58,342	104,091	1.952
PB-1/4D	21,508	112,479	12,988	13,750	22,048	110,088	103.384	2.581
PB-1/M4D	19,155	59,032	12,550	12,895	19,529	58,186	106,306	2.419

IV.1.2.3. Thermal characteristics

IV.1.2.3.1. Differential scanning calorimetry (DSC)

Samples weighing about 10 to 15 mg were scanned by a DSC at heating and cooling speeds of 10 °C/min in an inert atmosphere for the purpose of investigating the melting and crystallization temperatures, enthalpy energies, and degree of crystallinity. A total of three cycles were performed, starting with heating the samples from the ambient temperature to 180 °C, followed by a cooling cycle back to the ambient temperature before increasing it again up to 180 °C. The melting endotherms shown in **Fig IV. 5(a)** correspond to the melting of the neat PB-1 and PB-1/ Diatomaceous earth microcomposites both in the absence and presence of the RXR agent as obtained from the first heating cycle. The melting temperatures seem to remain constant at 140 °C in all cases, which corresponds to the melting temperature of the stable Form I [12–15]. The enthalpy of fusion was calculated from the integral of the area under the melting curve, while the degree of crystallinity was calculated using equation (1) [16]. The heat of fusion of 100% crystalline PB-1 is estimated to be 125 J/g for Form I [12, 17]. The addition of both the Diatomaceous earth and the RXR agent appeared to noticeably reduce both the melting enthalpy and the degree of crystallinity, as can be seen from the results in **Table IV.2**, which are attributed to the reduction of the crystalline phase, which means that both the Diatomaceous earth particles and the RXR hindered the formation of the crystalline phase. The exothermic curves generated from the cooling cycle seem to be altered in the case of the RXR-modified systems, as shown in **Fig IV. 5(b)**. The addition of Diatomaceous

earth seems to slow the crystallization process, as can be seen from the decrease in the crystallization temperature, whereas the addition of RXR agent had less effect on the crystallization temperature in comparison to the unmodified microcomposites. A similar effect was observed by the addition of small ratios of iPP to the PB-1 resin, as found in another study [18]. The melting endotherms from the third cycle showed a constant melting temperature around of 120 °C in both cases as illustrated in **Fig IV. 5(c)** and **Table IV.2**, which correspond to the melting of the unstable Form II [12–14]. The heat of fusion of Form II is around 71.1 J/g [12, 17] and the degree of crystallinity was calculated using the same equation used above. PB-1 possesses the least crystallinity degree while in Form II, since it takes quite a time to transform to Form I from the melt cooling.

$$X_c = \Delta H_m / ((1-w) \times \Delta H_{m100\%}) \ldots\ldots\ldots\ldots (1)$$

X_c: Degree of crystallinity

w: Weight fraction of Diatomaceous earth in the polymer matrix

$\Delta H_{m100\%}$: Heat of fusion of 100% crystalline PB-1

ΔH_m: Measured heat of fusion

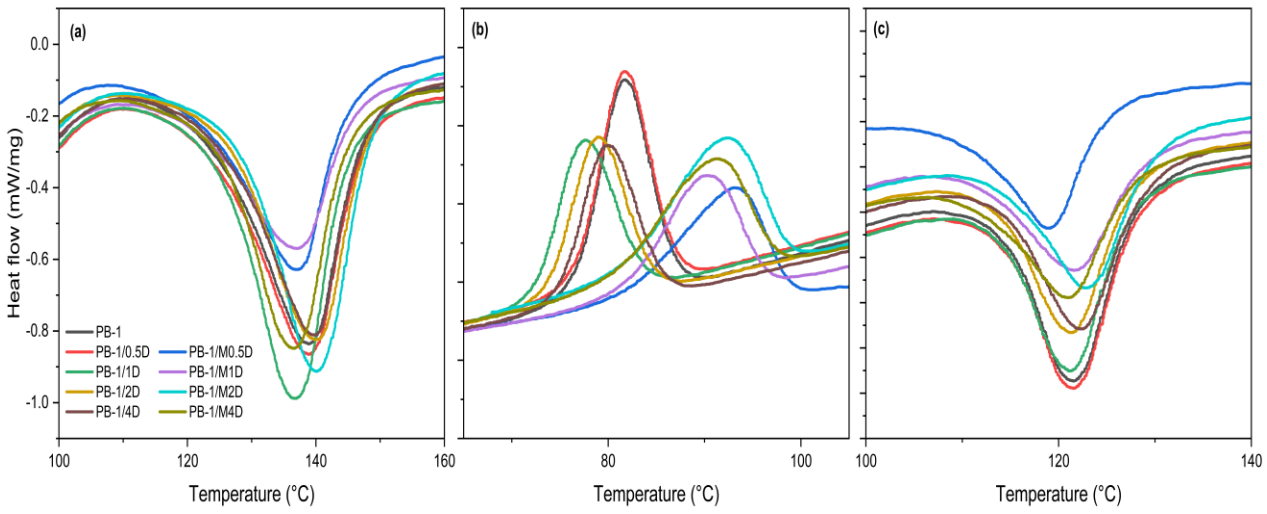

Fig IV. 5. DSC thermograms of the neat PB-1, PB-1/Diatomaceous earth and RXR modified PB-1/ Diatomaceous earth microcomposites at: **(a)** First melting cycle, **(b)** crystallization and **(c)** second melting cycle.

Table IV.2. DSC results summery of the Diatomaceous earth filled PB-1 with and without the RXR agent.

	T_{m1} (°C)	T_{m2} (°C)	ΔH_{m1} (J.g^{-1})	ΔH_{m2} (J.g^{-1})	T_c (°C)	ΔH_c (J.g^{-1})	X_{c1} (%)	X_{c2} (%)
PB-1	140	122	83	36	104	37	77	51
PB-1/0.5D	139	122	62	27	82	22	71	38
PB-1/M0.5D	137	119	53	18	93	19	61	25
PB-1/1D	137	121	67	22	76	17	77	31
PB-1/M1D	137	119	45	19	93	17	51	27
PB-1/2D	140	122	60	22	79	17	69	32
PB-1/M2D	140	123	63	19	92	22	72	27
PB-1/4D	140	123	57	21	80	16	67	31
PB-1/M4D	136	121	58	19	91	19	69	28

IV.1.2.3.2. Thermogravimetric analysis (TGA)

The thermal stability of the neat PB-1 and PB-1/Diatomaceous earth microcomposites, both in the absence and presence of the RXR agent, was investigated using a thermogravimetric analysis under an inert atmosphere. **Fig IV. 6** presents the thermal stability of the neat PB-1 and the studied microcomposites as shown by the weight loss measurement and the decomposition rate illustrated by its derivative plotting. From the figure, it's obviously clear that the addition of both Diatomaceous earth and RXR agent to the mixtures greatly improved the thermal stability of PB-1 resin. With a decomposition onset temperature of about 353 °C, neat PB-1 is considered to be a thermally stable polymer [17]. While, with the addition of the filler and the RXR agent into the mixtures, the thermal endurance of the PB-1 enhanced even more, reaching a decomposition onset temperature of about 435 °C. Several studies have found that Diatomaceous earth filler has a positive effect on the thermal stability of polymers [19–21]. From the DTG measurements, the temperature at the highest decomposition was recorded to reach 460 °C, and the decomposition rate was multiplied nearly three times, as shown in **Table IV.3**.

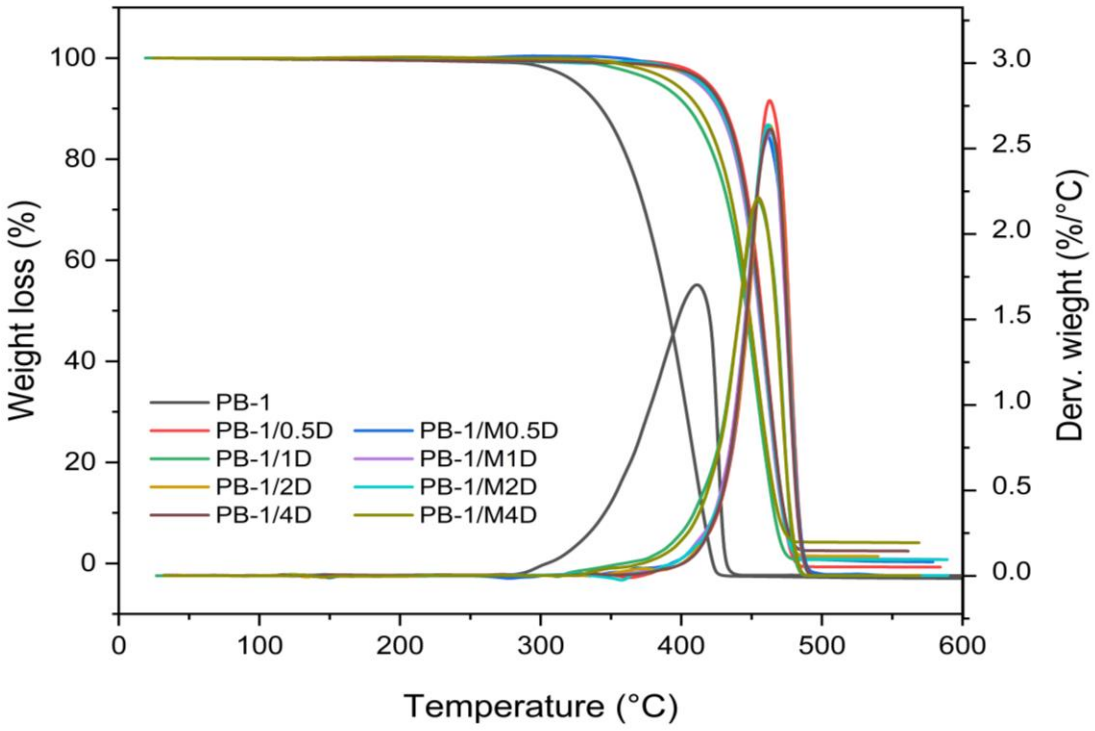

Fig IV. 6. TGA thermogram of neat PB-1 and both RXR modified and unmodified PB-1/Diatomaceous earth microcomposites.

Table IV.3. TGA & DTG measurements of neat PB-1 and both RXR modified and unmodified PB-1/Diatomaceous earth microcomposites.

	TGA				**DTG**	
	T_0 (°C)	T_f (°C)	T_{50} (°C)	t (min)	T_{DTG} (°C)	dwt [%/min]
PB-1	353	423	390	38.88	408	17.11
PB-1/0.5D	434	475	457	21.76	462	59.17
PB-1/M0.5D	429	475	455	21.81	459	55.13
PB-1/1D	420	469	446	22.09	451	45.50
PB-1/M1D	432	474	455	22.04	464	54.74
PB-1/2D	435	475	456	21.94	462	55.31
PB-1/M2D	433	474	455	22.23	461	56.20
PB-1/4D	434	475	456	22.10	459	54.27
PB-1/M4D	423	469	448	21.98	455	46.46

IV.1.2.4. Structural and morphological properties

IV.1.2.4.1. Fourier transform infrared (FTIR)

The evolution of the different crystalline phases in both the RXR agent-modified and unmodified PB-1/Diatomaceous earth microcomposites was investigated by FTIR analysis. Different vibrational bands appeared in the scanned range from 400 to 4000 cm^{-1}, referring to the vibrational movements of the neat PB-1, Diatomaceous earth, and RXR agent, yet no chemical interactions were noticed. Nonetheless, since crystal modification is the main goal of this test and Form I and II are the most important crystal phases in PB-1, the scanning range was narrowed to the wavenumber of interest (700–1200 cm^{-1}). Conformational bands appeared at 1328, 1098, 1060, 1027, 1000, 924, 845, and 815 cm^{-1}, corresponding to Form I, and bands at 1111, 1049, 1001, and 908 cm^{-1}, corresponding to Form II, but for simplicity reasons, only bands at 908 and 924 cm^{-1} were monitored. From the spectrum in **Fig IV. 7**, one can see that neat PB-1 demonstrates a small distinctive band at 908 cm^{-1}, which corresponds to the metastable Form II [15, 17, 22] and the reason for this is that the PB-1 sample was not conditioned for a long period of time before it was analyzed by FTIR, which explains the absence of Form I. On the other hand, samples containing Diatomaceous earth and RXR agent show a distinctive peak at 924 cm^{-1}, which corresponds to Form I [15, 17, 22],while the band intensity decreases with the increase in Diatomaceous earth content, reflecting its hindering effect on crystallization.

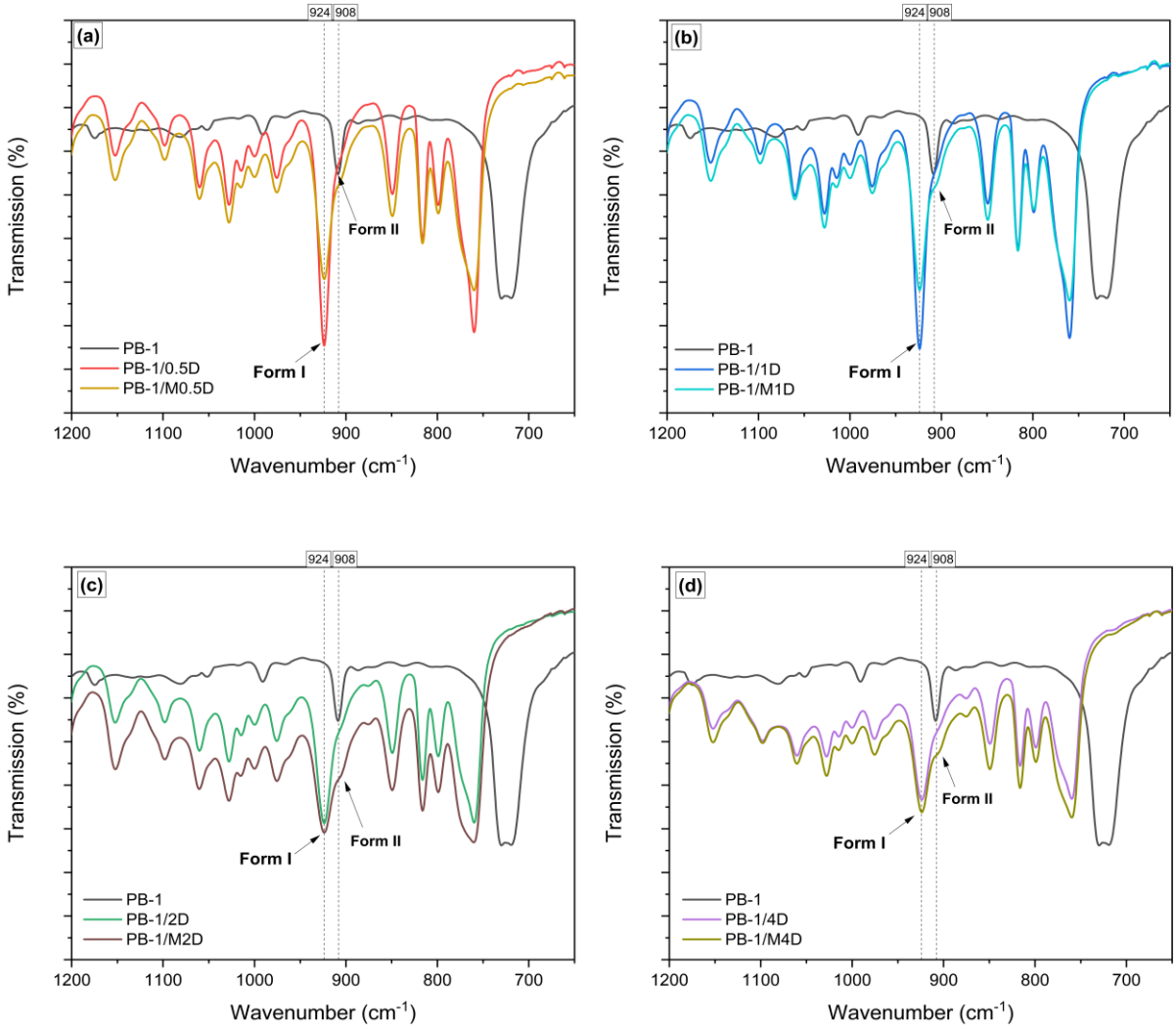

Fig IV. 7. FTIR spectrums of both RXR modified and unmodified PB-1/Diatomaceous earth microcomposites at: **(a)** 0.5wt %, **(b)** 1wt %, **(c)** 2wt % and **(d)** 4wt % of Diatomaceous earth content.

IV.1.2.4.2. Wide angle X-Ray scattering (WAXS)

The crystalline structure of the neat PB-1, PB-1/Diatomaceous earth, and RXR agent-modified PB-1/Diatomaceous earth microcomposites was analyzed by the WAXS test. From **Fig IV. 8**, neat PB-1 is characterized by three sharp peaks at an angle of 2θ = 9.7, 17, 20.26, and 20.51°, corresponding to the planes (110), (300), (220), and (211), respectively, which are the characteristic peaks of Form I. Another small peak with a plane structure (213) can be seen at 2θ = 17.8 °, referring to the presence of Form II [23]. The addition of both the Diatomaceous earth and the RXR agent into the mixtures seems to shift and reduce the intensity of the diffraction peaks, resulting in a change of both the crystal structure and the crystallinity, as illustrated in **Fig IV. 9**. As the RXR agent was

added to the mixtures, it was noticed that the peaks with the plane structures (200) and (213), related to Form II, seemed to diminish, and the peaks with the plane structures (110) and (300), corresponding to Form I, increased greatly. even though PB-1 shows a tetragonal crystal modification in all cases, which corresponds to the metastable Form II [13, 17, 24], as was calculated using an XRD analysis software, under the name "Match3," but the RXR agent seems to somehow had an effect on the transformation rate from Form II to Form I, which is in good agreement with the crystallization results found in the DSC.

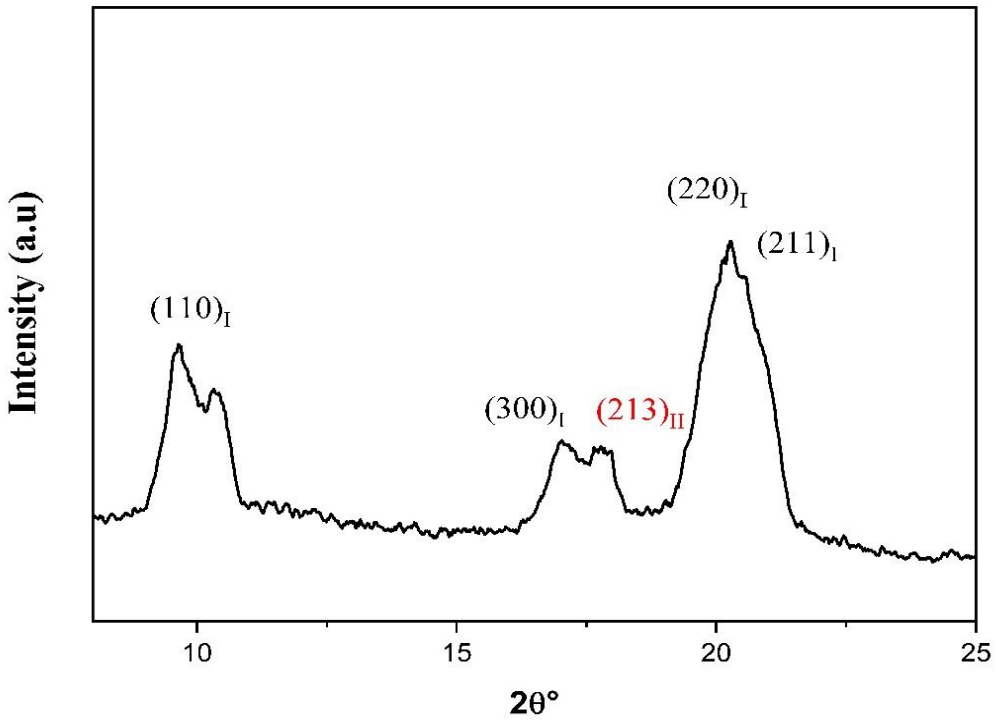

Fig IV. 8. WAXS diffraction peak of neat PB-1.

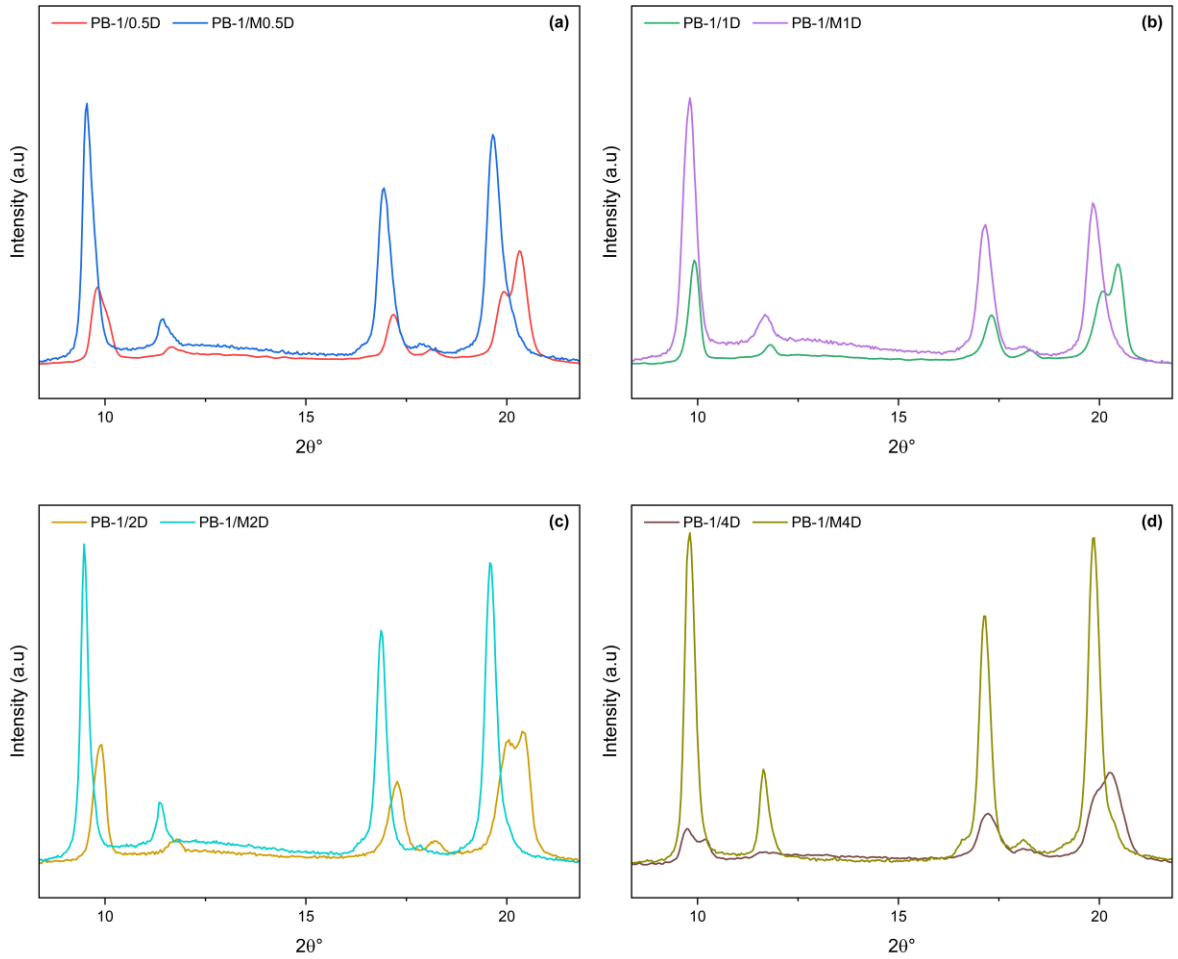

Fig IV. 9. WAXS spectrums of both RXR modified and unmodified PB-1/Diatomaceous earth microcomposites at: **(a)** 0.5 wt%, **(b)** 1 wt%, **(c)** 2 wt% and **(d)** 4 wt% of Diatomaceous earth content.

IV.1.2.4.3. Scanning electronic microscopy (SEM)

The morphology and filler dispersion and distribution within the PB-1 resin at different Diatomaceous earth contents were examined by the SEM analysis. **Fig IV. 10** (**a** and **b**) corresponds to the neat PB-1 resin, while figures (**c** and **d**) and (**c'** and **d'**) correspond to the filled PB-1 with 1 wt % Diatomaceous earth, both in the absence and presence of the RXR agent, respectively. Neat PB-1 shows a smooth surface texture with a clean fracture surface. From **Fig IV. 10(c)**, a bare Diatomaceous earth particle can be seen sitting in a hole, with no interfacial interactions between the particle and the resin itself, thus explaining the reduction in the mechanical properties and the tensile strength in particular. The distribution of the filler particles was not achieved, as can be seen from **Fig IV. 10 (d)**, which shows a large irregular particle, perhaps resulting from the agglomeration

of Diatomaceous earth particles. We noticed the same trend with the incorporation of the RXR agent as we did with Diatomaceous earth alone.

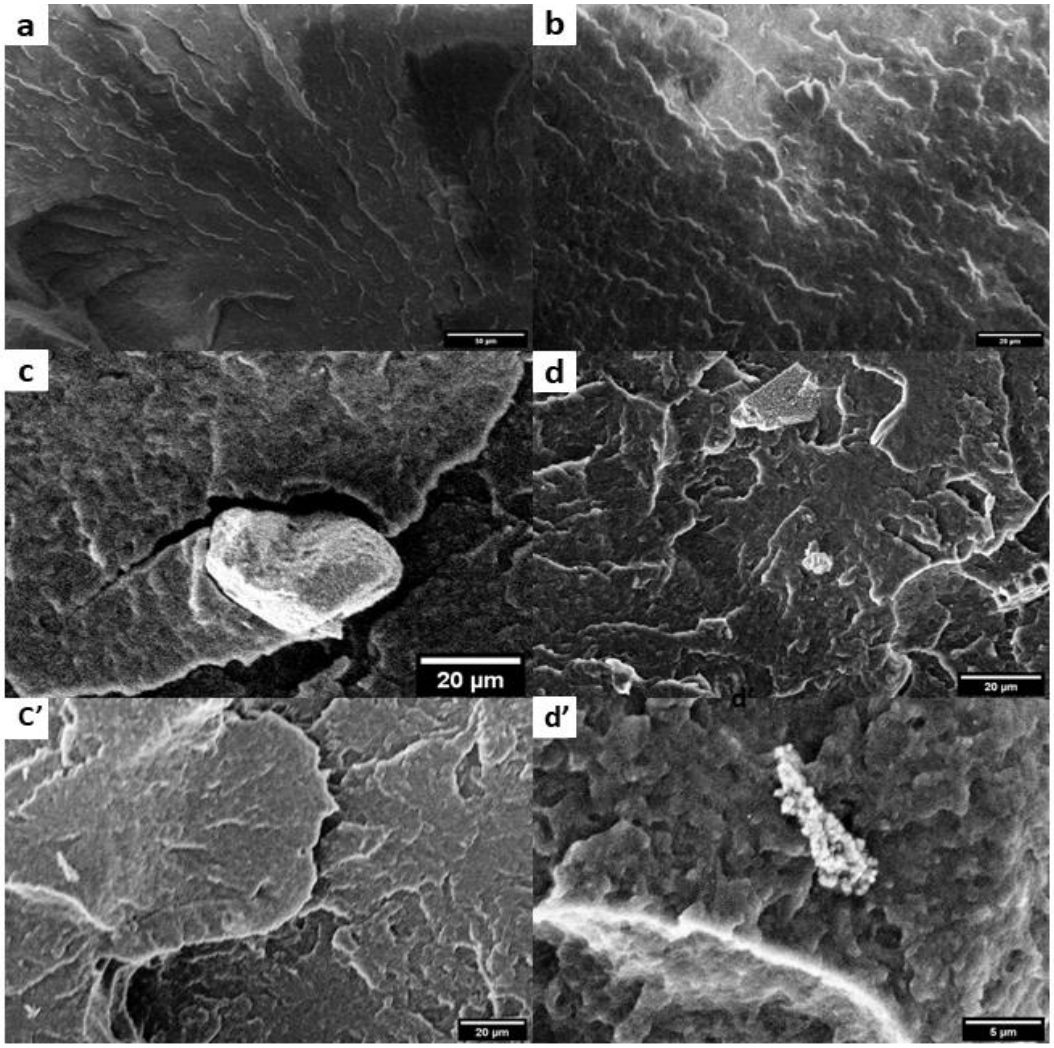

Fig IV. 10. SEM micrographs of the neat PB-1 (**a** and **b**) and PB-1/Diatomaceous earth microcomposites at 1 wt% Diatomaceous earth content, both in case of the unmodified (**c** and **d**) and the RXR modified samples (**c'** and **d'**).

References

[1] Saci, H.; Bouhelal, S.; Bouzarafa, B.; López, D.; Fernández-García, M. Reversible Crosslinked Low Density Polyethylenes: Structure and Thermal Properties. *Journal of Polymer Research* **2016**, *23* (4), 68. https://doi.org/10.1007/s10965-016-0965-x.

[2] Zhao, Y.; Ma, C.; Cheng, S.; Xu, W.; Du, Y.; Bao, Y.; Xiao, Z. Maleic Anhydride-Grafted Isotactic Polybutene-1 and Modified Polyamide 6. *Polymers (Basel)* **2018**, *10* (8), 1–12. https://doi.org/10.3390/polym10080872.

[3] Tariq, A.; Ahmad, N. M.; Abbas, M. A.; Shakir, M. F.; Khaliq, Z.; Rafiq, S.; Ali, Z.; Elaissari, A. Reactive Extrusion of Maleic-Anhydride-Grafted Polypropylene by Torque Rheometer and Its Application as Compatibilizer. *Polymers (Basel)* **2021**, *13* (4), 495. https://doi.org/10.3390/polym13040495.

[4] Bouhelal, S.; Cagiao, M. E.; Benachour, D.; Calleja, F. J. B. Structure Modification of Isotactic Polypropylene through Chemical Crosslinking: Toughening Mechanism. *J Appl Polym Sci* **2007**, *103* (5), 2968–2976. https://doi.org/10.1002/app.25406.

[5] Khellaf, S.; Khoffi, F.; Tabet, H.; Lallam, A.; Bouhelal, S.; Cagiao, M. E.; Benachour, D.; BaltáCalleja, F. J. Study of IPP Crosslinking by Means of Dynamic and Steady Rheology Measurements. *J Appl Polym Sci* **2012**, *124* (4), 3184–3191. https://doi.org/10.1002/app.34996.

[6] Bouhelal, S.; Cagiao, M. E.; Di Lorenzo, M. L.; Zouai, F.; Khellaf, S.; Tabet, H.; Benachour, D.; Calleja, F. J. B. Study of Rheological and Mechanical Properties of Ternary Blends of IPP/LDPE/EPDM. *Journal of Polymer Engineering* **2012**, *32* (3). https://doi.org/10.1515/polyeng-2011-0130.

[7] Afrifah, K. A.; Hickok, R. A.; Matuana, L. M. Polybutene as a Matrix for Wood Plastic Composites. *Compos Sci Technol* **2010**, *70* (1), 167–172. https://doi.org/10.1016/j.compscitech.2009.09.019.

[8] Abu-Zurayk, R.; Hamadneh, I.; Al-Dujaili, A. H. Preparation and Characterization of Polyethylene/Cellulose Composite with Diatomite and Bentonite as Fillers. *Polymer-Plastics Technology and Materials* **2020**, *59* (5), 546–554. https://doi.org/10.1080/25740881.2019.1669652.

[9] Sever, K.; Atagur, M.; Altay, L.; Seki, Y.; Uysalman, T.; Sen, I.; Kaya, N.; Guven, A.; Sarikanat, M. Effect of Diatomite Weight Fraction on Morphology, Thermal and Physical Properties of Diatomite Filled High Density Polyethylene Composites. *Acta Phys Pol A* **2018**, *134* (1), 281–284. https://doi.org/10.12693/APhysPolA.134.281.

[10] Aguero, A.; Quiles-Carrillo, L.; Jorda-Vilaplana, A.; Fenollar, O.; Montanes, N. Effect of Different Compatibilizers on Environmentally Friendly Composites from Poly(Lactic Acid) and Diatomaceous Earth. *Polym Int* **2019**, *68* (5), 893–903. https://doi.org/10.1002/pi.5779.

[11] Wu, G.; Ma, S.; Bai, Y.; Zhang, H. The Surface Modification of Diatomite, Thermal, and Mechanical Properties of Poly(Vinyl Chloride)/Diatomite Composites. *Journal of Vinyl and Additive Technology* **2019**, *25*, E39–E47. https://doi.org/10.1002/vnl.21664.

[12] Wanjale, S. D.; Jog, J. P. Poly (1-Butene)/Clay Nanocomposites: A Crystallization Study. *J Macromol Sci Phys* **2003**, *42* B (6), 1141–1152. https://doi.org/10.1081/MB-120024810.

[13] Hu, D.; Li, W.; Wu, K.; Cui, L.; Xu, Z.; Zhao, L. Utilization of Supercritical CO2 for Controlling the Crystal Phase Transition and Cell Morphology of Isotactic Polybutene-1 Foams. *Journal of CO2 Utilization* **2022**, *66*, 102265. https://doi.org/10.1016/j.jcou.2022.102265.

[14] Deepali Kulkarni, Dr. Jyoti. P. J. Effect of Nano Silica on Phase Transformation from Form-II to Form –I of Polybutene-1. *International Research Journal of Engineering and Technology (IRJET)* **2020**, *07* (11), 4.

[15] Wei, X.; Qu, Y.; Jiang, H.; Huang, Z.-X.; Qu, J.-P. Melt-State Dynamic Pressure Engineered Polybutene-1 with Form I Crystals. *Polymer (Guildf)* **2022**, *256*, 125185. https://doi.org/10.1016/j.polymer.2022.125185.

[16] Tarani, E.; Arvanitidis, I.; Christofilos, D.; Bikiaris, D. N.; Chrissafis, K.; Vourlias, G. Calculation of the Degree of Crystallinity of HDPE/GNPs Nanocomposites by Using Various Experimental Techniques: A Comparative Study. *J Mater Sci* **2023**, *58* (4), 1621–1639. https://doi.org/10.1007/s10853-022-08125-4.

[17] Abedi, S.; Sharifi-Sanjani, N. Preparation of High Isotactic Polybutene-1. *J Appl Polym Sci* **2000**, *78* (14), 2533–2539. https://doi.org/10.1002/1097-4628(20001227)78:14<2533::AID-APP140>3.0.CO;2-U.

[18] Liang, A.; Li, J.; Jiang, S. Role of Amorphous Phase in II-I Transition of IPB-1/IPP Blends. *Polymer (Guildf)* **2024**, *296*, 126818. https://doi.org/10.1016/j.polymer.2024.126818.

[19] Gonzalez, L.; Agüero, A.; Quiles-Carrillo, L.; Lascano, D.; Montanes, N. Optimization of the Loading of an Environmentally Friendly Compatibilizer Derived from Linseed Oil in Poly(Lactic Acid)/Diatomaceous Earth Composites. *Materials* **2019**, *12* (10), 1–15. https://doi.org/10.3390/ma12101627.

[20] Wang, K. Y.; Sun, Q. J.; Liu, Y.; Lu, J. Thermal Behavior, Mechanical Property and Microstructure of Low-Density Polyethylene Filled by Diatomite. *Applied Mechanics and Materials* **2014**, *633–634*, 413–416. https://doi.org/10.4028/www.scientific.net/AMM.633-634.413.

[21] Zhan, F.; Chen, N. C.; Zhang, X. H.; Huang, B.; Wu, Z. N.; Zhu, Q. Abrasion Properties and Thermal Stabilities of Poly(Vinylchloride)/Diatomite Composites. *Adv Mat Res* **2014**, *833*, 317–321. https://doi.org/10.4028/www.scientific.net/AMR.833.317.

[22] Zhang, Z.; Chen, X.; Zhang, C.; Liu, C.-T.; Wang, Z.; Liu, Y.-P. Polymorphic Transition of Pre-Oriented Polybutene-1 under Tensile Deformation: In Situ FTIR Study. *Chinese Journal of Polymer Science* **2020**, *38* (8), 888–897. https://doi.org/10.1007/s10118-020-2367-6.

[23] Ma, Y.-P.; Zheng, W.-P.; Liu, C.-G.; Shao, H.-F.; Nie, H.-R.; He, A.-H. Differential Polymorphic Transformation Behavior of Polybutene-1 with Multiple Isotactic Sequences. *Chinese Journal of Polymer Science* **2020**, *38* (2), 164–173. https://doi.org/10.1007/s10118-020-2337-6.

[24] Kaszonyiova, M.; Rybnikar, F. Influence of the Environment on the Phase II - I Transformation of Isotactic Polybutene-1. *Journal of Macromolecular Science, Part B: Physics* **2019**, *58* (2), 248–262. https://doi.org/10.1080/00222348.2019.1574424.

GENERAL CONCLUSION AND PERSPECTIVES

GENERAL CONCLUSION AND PERSPECTIVES

Throughout the course of this thesis, a comprehensive investigation into the effects of Diatomaceous earth and a newly developed RXR agent on the properties of HDPE and PB-1 based composites has been conducted. The research has shed light on the potential of these additives to modify the thermal, rheological, mechanical, structural, and morphological characteristics of the polymer matrices, offering valuable insights into their application in various industrial contexts.

Through the investigations carried out using different characterization techniques, Diatomaceous earth filler was found to have no effect on the final viscosity of the molten resins at lower concentrations, making it a more practical in processing techniques requiring lower viscosity, like the injection molding process. Moreover, the mechanical properties, represented by both the tensile and impact resistance, were negatively affected due the lack of interfacial interactions filler-matrix as was observed from the SEM micrographs. Stiffness of both HDPE and PB-1 composites, were noticed to decrease with the incorporation of the diatomaceous earth, giving its low stiffness, porosity and pseudo-lubricating effect. Melting temperatures didn't seem to be affected with the addition of the diatomaceous earth filler in both resins, while, the melting enthalpy of HDPE as well as the crystallinity degree and the crystal size were increased, reflecting the nucleating effect that the filler played in the matrix. PB-1 on the other hand, was negatively affected in term of the crystallization temperature, crystallization enthalpy and crystallinity degree, when the diatomaceous earth was included into the mixture, showing a hindering effect on the crystallization properties. The thermal endurance is another important factor that was greatly altered in the case of PB-1, where a very noticeable enhancement was noticed with the diatomaceous earth addition, while in HDPE case, no change was recorded. FTIR spectra, revealed that there were no chemical interactions were formed between the filler and the matrix resin, which explains the decrease in the mechanical properties. Nonetheless, it was observed that the inclusion of both the RXR and the filler into

the PB-1 has indeed a hindering effect on the crystallization as was seen from the DSC results. WAXS measurements were in good agreement with the DSC results, concerning the crystallinity degree, while the crystallite structure remained unaffected.

The incorporation of the RXR agent has induced a crosslinking reaction in both systems as revealed from the DRA results, and also showed a positive effect on the dispersion of the diatomaceous earth particles, powered by the high torque generated from crosslinking reaction.

Moreover, the research conducted as part of this thesis emphasizes the necessity for further investigation aimed at addressing the identified challenges. Specifically, efforts should focus on optimizing the compatibility of Diatomaceous earth with polymer matrices to enhance filler-matrix interactions, and further investigating the effect of varying concentrations of the RXR agent on the two systems and the conversion rate of PB-1 from Form II to Form I in particular. The filler's particle size and surface treatment are also important parameters that could investigated in detail, to fully explore the potential of the diatomaceous earth filler.

Comprehensive analyses utilizing advanced techniques, including Dynamic Rheological Analysis, Differential Scanning Calorimetry, Thermogravimetric Analysis, Wide-angle X-ray Scattering, Fourier Infrared Transform, and Scanning Electron Microscope imaging, have provided invaluable insights into the effects of these additives on the properties of polymer composites.

Abstract

This study explores the influence of a novel reversible crosslinking reaction agent (RXR) and Diatomaceous earth on the properties of two distinct polymers: high-density polyethylene (HDPE) and isotactic polybutene-1 (PB-1). Reactive extrusion with a the unique RXR agent was used to create microcomposites with both unmodified and modified DE. A comprehensive analysis using dynamic rheological analysis (DRA), tensile and impact tests, differential scanning calorimetry (DSC), thermogravimetric analysis (TGA), wide-angle X-ray scattering (WAXS), Fourier transform infrared spectroscopy (FTIR), and scanning electron microscopy (SEM) was conducted. The results revealed contrasting effects on the two polymers. In HDPE, Diatomaceous earth alone decreased mechanical performance due to aggregation, but surprisingly enhanced crystallinity. The RXR agent improved HDPE's tensile and impact strengths through crosslinking, but lowered crystallinity. Conversely, in PB-1, the RXR agent increased viscosity while Diatomaceous earth displayed minimal rheological impact. However, the combined addition of Diatomaceous earth and RXR significantly reduced PB-1's mechanical properties and increased the crystallization temperature. Thermal stability improved with Diatomaceous earth in both polymers. FTIR and WAXS analysis indicated minimal changes in crystalline structure for both additives in either polymer. SEM micrographs revealed Diatomaceous earth clustering in, suggesting weak filler-matrix interactions, which likely explains the observed decrease in mechanical properties.

Keywords: High Density-Polyethylene (HDPE), Isotactic Polybutene-1 (PB-1), RXR, Microcomposites, Diatomaceous earth.

Résumé :

Cette étude explore l'influence d'un nouvel agent de réticulation réversible (RXR) et de la diatomite sur les propriétés de deux polymères distincts : le polyéthylène haute densité (HDPE) et le polybutène isotatique-1 (PB-1). L'extrusion réactive avec un agent RXR unique a été utilisée pour créer des microcomposites à la fois avec diatomite non modifiée et modifié. Une analyse complète a été réalisée à l'aide de l'analyse rhéologique dynamique (DRA), des tests de traction et de choc, de la calorimétrie différentielle à balayage (DSC), d'une analyse thermogravimétrique (TGA), de la dispersion à large angle des rayons X (WAXS), du spectroscope infrarouge de transformation de Fourier (FTIR) et de la microscopie électronique à balayage (SEM). Les résultats ont révélé des effets contrastants sur les deux polymères. Dans le HDPE, la diatomite seule a diminuée les performances mécaniques en raison de l'agrégation, mais a amélioré la cristallinité de façon surprenante. L'agent RXR a amélioré les forces de traction et d'impact de l'HDPE par la réticulation, mais a réduit la cristallinité. À l'inverse, dans le PB-1, l'agent RXR a augmenté la viscosité tandis que la diatomite a montré un impact rhéologique minimal. Toutefois, l'ajout combiné de diatomite et de RXR a considérablement réduit les propriétés mécaniques de PB-1 et a augmenté la température de cristallisation. La stabilité thermique s'est améliorée avec la diatomite dans les deux polymères. Les analyses FTIR et WAXS ont montré des changements minimes dans la structure cristalline des deux additifs dans les deux polymères. Les micrographes SEM ont révélé le regroupement de diatomite, suggérant des interactions faibles entre la charge et la matrice, ce qui explique probablement la diminution observée des propriétés mécaniques.

Mots-clés : Polyéthylène haute densité (HDPE), Polybutène isotactique-1 (PB-1), RXR, Microcomposites, diatomite.

الملخص:

تستكشف هذه الدراسة تأثير عامل تفاعل تشابك عكسي جديد (RXR) والتراب الدياتومي (DE) على خواص اثنين من البوليمرات المتميزة: البولي إيثيلين عالي الكثافة (HDPE) والبولي بيوتيني متساوي التباين-1 (PB-1). استُخدم البثق التفاعلي مع عامل RXR الفريد من نوعه لإنشاء مركبات مجهرية مع كل من البولي إيثيلين عالي الكثافة غير المعدل والمعدل. تم إجراء تحليل شامل باستخدام التحليل الانسيابي الديناميكي (DRA)، واختبارات الشد والصدمات، وقياس السعرات الحرارية بالمسح التفاضلي (DSC)، والتحليل الحراري الوزني (TGA)، والتشتت واسع الزاوية بالأشعة السينية (WAXS)، والتحليل الطيفي بالأشعة تحت الحمراء المحولة فورييه (FTIR)، والفحص المجهري الإلكتروني الماسح (SEM). كشفت النتائج عن تأثيرات متباينة على البوليمرين. في البولي إثيلين عالي الكثافة (HDPE)، انخفض الأداء الميكانيكي في البولي إثيلين عالي الكثافة وحده بسبب التجميع، ولكنه عزز التبلور بشكل مدهش. وحسّن عامل RXR قوة الشد والصدمات في البولي إثيلين عالي الكثافة من خلال التشابك المتبادل، لكنه قلل من التبلور. وعلى العكس من ذلك، في PB-1، زاد عامل RXR من اللزوجة في حين أظهر DIATOMACEOUS EARTH تأثيرًا انسيابيًا ضئيلًا. ومع ذلك، فإن إضافة DE وRXR معًا قلل بشكل كبير من الخواص الميكانيكية ل PB-1 وزاد من درجة حرارة التبلور. تحسن الاستقرار الحراري مع DIATOMACEOUS EARTH في كلا البوليمرين. أشار تحليل FTIR وتحليل WAXS إلى الحد الأدنى من التغييرات في التركيب البلوري لكلا المضافين في كلا البوليمرين. كشفت الصور المجهرية SEM عن تكتل DE، مما يشير إلى تفاعلات ضعيفة بين الحشو والمصفوفة، وهو ما يفسر على الأرجح الانخفاض الملحوظ في الخواص الميكانيكية

الكلمات الدلالية: بولي إيثيلين عالي الكثافة (HDPE)، بولي بيوتين أيزوتاكتيك-1 (PB-1)، RXR، مركبات ميكروكمبوسايت.